Monthly Notices of the ROYAL ASTRONOMICAL SOCIETY

MNRAS **533,** 1907–1926 (2024) https://doi.org/10.1093/mnras/stae1819
Advance Access publication 2024 July 27

# Growth of high-redshift supermassive black holes from heavy seeds in the BRAHMA cosmological simulations: implications of overmassive black holes

Aklant K. Bhowmick [1]★, Laura Blecha,[1] Paul Torrey [2], Rachel S Somerville,[3] Luke Zoltan Kelley [4], Mark Vogelsberger [5], Rainer Weinberger [6], Lars Hernquist[7] and Aneesh Sivasankaran [1]

[1]*Department of Physics, University of Florida, Gainesville, FL 32611, USA*
[2]*Department of Astronomy, University of Virginia, Charlottesville, VA 22904, USA*
[3]*Center for Computational Astrophysics, Flatiron Institute, New York, NY 10010, USA*
[4]*Department of Astronomy, University of California at Berkeley, Berkeley, CA 94720, USA*
[5]*Department of Physics, Kavli Institute for Astrophysics and Space Research, Massachusetts Institute of Technology, Cambridge, MA 02139, USA*
[6]*Leibniz Institute for Astrophysics Potsdam (AIP), An der Sternwarte 16, D-14482 Potsdam, Germany*
[7]*Harvard-Smithsonian Center for Astrophysics, 60 Garden Street, Cambridge, MA 02138, USA*

Accepted 2024 July 24. Received 2024 July 24; in original form 2024 June 19

## ABSTRACT

*JWST* has revealed a large population of accreting black holes (BHs) in the early Universe. Recent work has shown that even after accounting for possible systematic biases, the high-$z$ $M_*$–$M_{\rm bh}$ relation can be above the local scaling relation by $> 3\sigma$. To understand the implications of these overmassive high-$z$ BHs, we study the BH growth at $z \sim 4$–7 using the [18 Mpc]$^3$ BRAHMA cosmological simulations with systematic variations of heavy seed models that emulate direct collapse black hole (DCBH) formation. In our least restrictive seed model, we place $\sim 10^5$ M$_\odot$ seeds in haloes with sufficient dense and metal-poor gas. To model conditions for direct collapse, we impose additional criteria based on a minimum Lyman Werner flux (LW flux $= 10\ J_{21}$), maximum gas spin, and an environmental richness criterion. The high-$z$ BH growth in our simulations is merger dominated, with a relatively small contribution from gas accretion. The simulation that includes all the above seeding criteria fails to reproduce an overmassive high-$z$ $M_*$–$M_{\rm bh}$ relation consistent with observations (by factor of $\sim 10$ at $z \sim 4$). However, more optimistic models that exclude the spin and environment based criteria are able to reproduce the observed relations if we assume $\lesssim 750$ Myr delay times between host galaxy mergers and subsequent BH mergers. Overall, our results suggest that current *JWST* observations may be explained with heavy seeding channels if their formation is more efficient than currently assumed DCBH conditions. Alternatively, we may need higher initial seed masses, additional contributions from lighter seeds to BH mergers, and / or more efficient modes for BH accretion.

**Key words:** methods: numerical – galaxies: evolution – galaxies: formation – (galaxies:) quasars: supermassive black holes.

## 1 INTRODUCTION

The *JWST* is transforming the observational landscape of supermassive black holes (SMBHs). Prior to *JWST*, the observed black hole (BH) population at high redshifts ($z \sim 4$–7.5) was confined to the most luminous quasars powered by BHs between $\sim 10^9$–$10^{10}$ M$_\odot$ (Fan et al. 2001; Willott et al. 2010; Mortlock et al. 2011; Venemans et al. 2015; Bañados et al. 2016, 2018; Jiang et al. 2016; Reed et al. 2017; Matsuoka et al. 2018, 2019; Wang et al. 2018, 2021; Yang et al. 2019). *JWST* is pushing these frontiers by revealing a large population of fainter broad line (BL) active galactic nucleus (AGN) candidates at $z \sim 4$–11 (Greene et al. 2024; Harikane et al. 2023; Kocevski et al. 2023; Larson et al. 2023; Maiolino et al. 2023; Onoue et al. 2023; Akins et al. 2024; Andika et al. 2024; Kocevski et al. 2024). About $\sim 20$ per cent of these BL AGNs are compact and heavily obscured, characterized by a steep red continuum in the rest frame optical along with relatively blue colours in the rest-frame UV (Greene et al. 2024; Harikane et al. 2023; Killi et al. 2023; Kocevski et al. 2023; Maiolino et al. 2023; Kokorev et al. 2024). These objects are now commonly referred to as 'Little red dots' or LRDs (Matthee et al. 2024). Greene et al. (2024) used follow-up NIRSpec/PRISM spectroscopy to demonstrate that $> 80$ per cent of LRDs in the UNCOVER sample contain AGN signatures in the form of broad emission lines after the brown dwarf contaminants are excluded (Langeroodi & Hjorth 2023).

For the spectroscopically confirmed AGNs, BH masses can be estimated based on the widths of the H $\alpha$ emission line, with measurements ranging from $\sim 10^6$–$10^8$ M$_\odot$ (Harikane et al. 2023; Kocevski et al. 2023; Larson et al. 2023; Maiolino et al. 2023; Onoue et al. 2023; Übler et al. 2023). Concurrently, the unprecedented resolution and sensitivity of NIRCam imaging has also made it possible to detect the starlight from the host galaxies of some high-$z$ BHs (Ding et al. 2023; Stone et al. 2024; Yue et al. 2024). By fitting the resulting SEDs while accounting for the contributions from AGN, it has been possible to also measure the stellar masses of the host galaxies. All these developments have resulted in the

★ E-mail: aklant.app@gmail.com

first ever measurements of the $M_*$ versus $M_{\rm bh}$ relations at $z \gtrsim 4$. Remarkably, the BH mass and host stellar mass measurements (albeit with large uncertainties at present) indicate the possible existence of a substantial population of 'overmassive' BHs that are $\sim$ 10–100 times heavier than expectations from local BH scaling relations (Kokorev et al. 2023; Bogdán et al. 2024; Durodola, Pacucci & Hickox 2024; Kocevski et al. 2024; Kokorev et al. 2024; Natarajan et al. 2024).

Despite these exciting developments, we still need to be cautious as the BH masses may be overestimated if for example, a portion of broadening in the emission lines is due to galactic-scale outflows (Richards et al. 2011; Denney 2012). At the same time, it is possible that the stellar masses are underestimated as it is often difficult to separate the stellar and AGN components in the SED (Ramos Padilla et al. 2020). However, since these LRDs have been shown to be extremely compact (Baggen et al. 2023), adding more stellar mass to the current estimates would lead to a further increase in the stellar densities that are already incredibly high. Relatedly, Pérez-González et al. (2024) has recently used the MIRI-SMILES data to show that the LRD SED shapes may also be explained by compact starburst galaxies along with some (subdominant) contribution from an AGN. Finally, even if the BH masses and host galaxy stellar masses are not *systematically* biased, we may still be observing a biased population of BHs living in significantly smaller galaxies than the *intrinsic*$M_*$ versus $M_{\rm bh}$ and the $M_*$ versus $L_{\rm bol}$ (AGN bolometric luminosity) relation. This bias is a consequence of the steep low-mass end of the underlying galaxy stellar mass function combined with the detection limits of surveys, and is referred to as *Lauer bias* (Lauer et al. 2007). As a result of Lauer Bias, the observed BHs are prone to be significantly higher than the intrinsic $M_*$ versus $M_{bh}$ relation. In addition to the Lauer bias, AGN time variability and the detection limit can together lead to Eddington bias; i.e. the preferential detection of AGNs at luminosities higher than the *time-averaged* values. While BH mass measurements may be less prone to Eddington bias than the luminosities, they may still be impacted if the luminosity of the broad emission line (used for the BH mass measurement) is also time variable. Pacucci et al. (2023) showed that despite the possible systematic biases as well as measurement uncertainties, the $M_*$ versus $M_{\rm bh}$ measurements (as they currently stand) of the spectroscopically confirmed AGNs still imply an intrinsic high-$z$ $M_*$ versus $M_{\rm bh}$ relation that is above the local scaling relations at the $> 3\sigma$ confidence level. However, Li et al. (2024) did a similar analysis of systematic biases and concluded that the intrinsic mean high-$z$ relation is consistent with the local scaling relations (but the scatter is $\sim$ 2 times higher). All these developments imply that despite these *JWST* measurements, it is still not firmly established whether high-$z$ BH populations are indeed overmassive compared to their local counterparts. Overall, while we are still in the earliest stages of characterizing the high-$z$ AGN populations, it is clear that *JWST* is well is on its way towards revolutionizing our understanding of early BH growth.

Along with the brightest high-$z$ quasars discovered in the pre-*JWST* era, the possibility of overmassive high-$z$ BH populations is expected to have strong implications for BH seeding. Possible candidates for the first seeds of SMBHs include 'light seeds' ($\sim 10^2$–$10^3$ $M_\odot$) as Population III stellar remnants (Fryer, Woosley & Heger 2001; Madau & Rees 2001; Xu, Wise & Norman 2013; Smith et al. 2018), 'intermediate-mass seeds' ($\sim 10^3$–$10^4$ $M_\odot$) as remnants from runaway stellar and BH collisions in dense nuclear star clusters (Davies, Miller & Bellovary 2011; Lupi et al. 2014; Kroupa et al. 2020; Das et al. 2021a, b), and 'heavy seeds' ($\gtrsim 10^4$ $M_\odot$) as direct collapse black holes (DCBHs; Bromm & Loeb 2003; Begelman, Volonteri & Rees 2006; Regan, Johansson & Wise 2014; Latif, Schleicher & Hartwig 2016; Luo et al. 2018; Wise et al. 2019; Luo et al. 2020; Begelman & Silk 2023; Mayer et al. 2024). The heaviest DCBH seeds have long been considered to be too rare to explain the entirety of the observed SMBH populations. However, the presence of overmassive BHs was predicted to be one of their key observational signatures (Agarwal et al. 2013; Natarajan et al. 2017; Visbal & Haiman 2018; Scoggins, Haiman & Wise 2023; Natarajan et al. 2024; Scoggins & Haiman 2024). Therefore, these *JWST* detections have sparked a renewed interest in heavy DCBH seeding channels (Pacucci et al. 2023; Jeon et al. 2024).

In contrast to the light and intermediate-mass seeds that form within star-forming regions, the heavy DCBH seeds form when fragmentation and star formation is prevented during gravitational collapse of a gas cloud. Instead of fragmenting, the gas must undergo a nearly isothermal collapse at temperatures above $\sim 10^4$ K. In addition, large gas inflow rates ($\gtrsim 0.1$ $M_\odot yr^{-1}$ at a few tens of pc scales sustained for $\sim$ 10 Myr) are required to form a massive compact object (e.g. Begelman 2010; Hosokawa, Omukai & Yorke 2012; Hosokawa et al. 2013; Schleicher et al. 2013; Regan et al. 2020a; Haemmerlé et al. 2021). To keep the gas from cooling below $\sim 10^4$ K, we first need pristine environments to prevent efficient metal cooling. In addition, we also need to prevent cooling due to molecular hydrogen ($H_2$). This could be potentially achieved by destroying the $H_2$ with sufficient ultraviolet (UV) radiation in the Lyman–Werner (LW) band (11.2–13.5 eV) provided by nearby star-forming regions. However, the estimated values of the critical LW flux ($J_{\rm crit}$) are extremely high ($\gtrsim 1000$ $J_{21}$, where $J_{21} = 10^{-21}$ erg s$^{-1}$ cm$^{-2}$ Hz$^{-1}$sr$^{-1}$) according to radiation hydrodynamic simulations (Shang, Bryan & Haiman 2010) as well as one-zone chemistry models (Sugimura, Omukai & Inoue 2014; Wolcott-Green, Haiman & Bryan 2017). Several previous works have shown that these critical fluxes are exceedingly difficult to achieve, particularly in pristine gas environments with no prior star formation history (Dijkstra et al. 2008; Habouzit et al. 2016; Bhowmick et al. 2022a). In addition to molecular hydrogen cooling, having high angular momentum may also impede the gas from achieving the required inflow rates of $\gtrsim 0.1$ $M_\odot$ yr$^{-1}$. This further restricts the number of feasible sites for DCBH formation (Lodato & Natarajan 2006). However, in Bhowmick et al. (2022a), we showed that the supercritical LW flux requirement is generally much more restrictive compared to that of low gas spins.

More recently, it has been found that dynamical heating during major mergers can compete against $H_2$ cooling and significantly lower the critical LW flux requirement ($\sim 1 - 10$ $J_{21}$) compared to previous estimates (Wise et al. 2019; Regan et al. 2020b, c). Regan et al. (2020b) demonstrated that the combination of mild LW radiation and dynamical heating within metal-free haloes can lead to the formation of multiple BHs via direct gas collapse, with masses ranging from $\sim$ 300 to $10^4$ $M_\odot$. These BHs can eventually sink to the halo centres and merge with one another to form $\sim 10^5$ $M_\odot$ DCBHs, which is close to the seed mass used in several large cosmological simulations (e.g. Khandai et al. 2015; Nelson et al. 2015; Feng et al. 2016; Kaviraj et al. 2017; Tremmel et al. 2017). While the reduced critical LW fluxes can substantially improve the prospect of DCBH formation, they will still be limited to environments where major mergers occur. Therefore, while the possibility of overmassive high-$z$ BHs may hint at heavy seeding origins, it is yet to be determined whether the existing DCBH formation mechanisms are sufficient for explaining these BH populations.

Cosmological simulations allow us to predict the BH populations that assemble from a given seeding origin and directly compare

against observations. However, while many cosmological simulations resolve down to the postulated DCBH seed masses ($\sim 10^4$–$10^5$ $M_\odot$, see review by Vogelsberger et al. 2020a), they cannot resolve the underlying physics that leads to the direct collapse. As a result, many cosmological simulations simply seed $\sim 10^5$–$10^6$ $M_\odot$ BHs based on a halo or galaxy mass threshold (e.g. Di Matteo et al. 2012; Vogelsberger et al. 2014b; Khandai et al. 2015; Sijacki et al. 2015; Nelson et al. 2019a). With these prescriptions, the primary goal is not to emulate the specific conditions of DCBH formation but rather to capture the observational expectation that massive galaxies harbour SMBHs. Therefore, the main focus of these simulations has typically been on understanding the influence of SMBHs on the evolution of galaxies (Huang et al. 2018; Li et al. 2020), instead of the origins of the SMBHs themselves. Recently, several simulations have incorporated more realistic seeding prescriptions to emulate DCBH-forming criteria that are based on local gas properties. For example, Tremmel et al. (2017) and Bellovary et al. (2019) seed $\sim 10^5$ $M_\odot$ BHs if an individual gas element has sufficiently high density, low metallicity, and high temperatures. However, seeding solely based on individual gas cells could compromise the resolution convergence of seed formation (see fig. 10 of Taylor & Kobayashi 2015). The resolution convergence may be improved by the slightly modified approach taken by Jeon et al. (2024), which avoids the overproduction of seeds at higher resolutions by requiring the gas cells in the entire neighbourhood (SPH smoothing kernel) of the seed formation site to satisfy the seeding criteria (high density, low metallicity, and high temperatures).

As mentioned above, many cosmological simulations have modelled DCBH formation in environments with high gas densities and low gas metallicities. However, it is crucial also to consider other conditions that are potentially relevant for DCBH formation, including low gas angular momentum, sufficient LW radiation, and the presence of dynamical heating due to major mergers. To the best of our knowledge, currently there are no cosmological simulations that simultaneously consider all of the above conditions in their seed models. As a result, it is currently unclear how all these different conditions come together to impact the formation and growth of DCBHs and their ensuing feasibility in producing the overmassive *JWST* BHs. To further complicate matters, the growth of these DCBHs would also be impacted by their dynamics and gas accretion. Similar to seeding, all these different aspects of BH physics are also extremely challenging to model in cosmological simulations due to resolution limitations. Moreover, they may have a degenerate impact on BH growth. However, in order to disentangle the complex interplay between BH seeding, dynamics and accretion, it is often useful to first study them in isolation. To that end, in this work, we largely focus on exploring BH seeding within a fixed set of assumptions about BH accretion, feedback, and dynamics.

This paper introduces a set of multiple cosmological simulation boxes, wherein we systematically vary the seeding prescriptions while all other aspects of the galaxy formation (including BH dynamics and accretion) model are adopted from the `Illustris-TNG` simulation suite (Marinacci et al. 2018; Naiman et al. 2018; Nelson et al. 2018, 2019a; Springel et al. 2018; Pillepich et al. 2018b). We incrementally stack the different seeding conditions relevant for DCBH formation (i.e. high density, low metallicty, low gas angular momentum, sufficient LW radiation, rich environment), and study their impact on the resulting BH populations to compare against the *JWST* results. All the seeding conditions have been developed and thoroughly tested for numerical convergence in our previous series of papers using cosmological zoom simulations (Bhowmick et al. 2021, 2022a, 2024a). These new simulations are part of the `BRAHMA` simulation suite introduced in our previous paper (Bhowmick et al. 2024b). We envision `BRAHMA` to eventually become a large suite of simulations encompassing a wide range of possible scenarios for BH seeding. While Bhowmick et al. (2024b) focused on low-mass seed models that emulated Pop III or NSC seeding conditions, this paper focuses on heavy seed models that emulate DCBH seeding conditions.

The structure of this paper is as follows. Section 2 introduces the methods, including the basic simulation set-up and the detailed implementation of all the seeding criteria used. Section 3 describes the predictions of our different simulation boxes for the seed formation rates, AGN luminosity functions (LFs), merger rates, and finally the $M_*$–$M_{\rm bh}$ relations. Finally, Section 4 describes the main conclusions of our work.

## 2 METHODS

To run our simulations, we used the `AREPO` gravity + magnetohydrodynamic (MHD) solver (Springel 2010; Pakmor, Bauer & Springel 2011; Pakmor et al. 2016; Weinberger, Springel & Pakmor 2020). The gravity solver uses the PM Tree (Barnes & Hut 1986) and the evolution of the gas is described by the ideal MHD equations solved over a dynamic unstructured grid generated via a Voronoi tessellation of the domain. All the simulations are characterized by the Planck Collaboration XIII (2016) cosmology i.e. $\Omega_\Lambda = 0.6911$, $\Omega_{\rm m} = 0.3089$, $\Omega_{\rm b} = 0.0486$, $H_0 = 67.74\,{\rm km\,s^{-1}Mpc^{-1}}$, $\sigma_8 = 0.8159$, $n_{\rm s} = 0.9667$. Haloes are identified using the Friends-of-Friends (FOF) algorithm (Davis et al. 1985) with a linking length of 0.2 times the mean particle separation. Subhaloes are computed using the `SUBFIND` (Springel et al. 2001) algorithm.

### 2.1 Initial conditions

We run our simulations using two distinct types of initial conditions (ICs). Most of the paper will focus on simulations that adopt the usual approach wherein the ICs are generated from a random Gaussian field. These 'unconstrained' ICs are produced at $z = 127$ using `MUSIC` (Hahn & Abel 2011). These simulations have a comoving volume of $[18\ {\rm Mpc}]^3$ and $512^3$ dark matter (DM) particles. However, because these boxes are relatively small, they do not probe the entire range of galaxy masses detected by *JWST*. Therefore, we also run additional simulations where the ICs are 'constrained' to produce more overdense regions. These constrained ICs were generated at $z = 99$ using the ⟨0:sc ⟩gaussian-cR⟨/0:sc⟩ code (Ni, Di Matteo & Feng 2022) over a $[9\ {\rm Mpc}]^3$ volume and $360^3$ DM particles (see Ni et al. 2022; Bhowmick et al. 2022b for more details). As we shall see, even though the unconstrained simulations are slightly larger than the constrained simulations, the constrained simulations produce more massive galaxies as they simulate a much more overdense region (i.e. $4\sigma$ overdensity at a scale of 1 Mpc). We chose the number of DM particles and initial gas cells such that for all of our simulations, the resulting DM mass resolution is $1.5 \times 10^6$ $M_\odot$ and the gas mass resolution is $\sim 10^5$ $M_\odot$.

### 2.2 `Illustris-TNG` galaxy formation model

With the exception of BH seeding, the `BRAHMA` simulations essentially adopt all the features of its predecessor `IllustrisTNG` (TNG) simulation suite (Marinacci et al. 2018; Naiman et al. 2018; Nelson et al. 2018, 2019a; Pillepich et al. 2018b; Springel et al. 2018; see also Genel et al. 2018; Weinberger et al. 2018; Donnari et al. 2019; Habouzit et al. 2019; Pillepich et al. 2019; Nelson et al. 2019b; Rodriguez-Gomez et al. 2019; Torrey et al. 2019; Habouzit

et al. 2021; Übler et al. 2021). Here, we summarize the core features of the TNG model that are most consequential to the seeding of BHs.

The radiative cooling is implemented by including contributions from primodial species (H, $H^+$, He, $He^+$, $He^{++}$ based on Katz, Weinberg & Hernquist 1996) as well as metals. The metal cooling rates are interpolated from pre-calculated tables as in Smith, Sigurdsson & Abel (2008) in the presence of a spatially uniform, time-dependent UV background. The cooling of gas leads to the formation of dense gas, wherein star formation occurs at densities exceeding 0.13 $cm^{-3}$ with a time-scale of 2.2 Gyr. The star-forming gas cells represent an unresolved multiphase interstellar medium described by an effective equation of state (Springel & Hernquist 2003; Vogelsberger et al. 2014a). Star particles represent unresolved single stellar populations that are characterized by their ages and metallicities. The underlying initial mass function is adopted from Chabrier (2003). The subsequent stellar evolution is modelled based on Vogelsberger et al. (2013) with modifications for IllustrisTNG as described in Pillepich et al. (2018a). The stellar evolution leads to chemical enrichment of stars, which is modelled by following the evolution of seven species of metals (C, N, O, Ne, Mg, Si, Fe) in addition to H and He. Stellar and Type Ia/II Supernova feedback are modelled as galactic scale winds (Pillepich et al. 2018b) that deposit mass, momentum and metals on to the gas surrounding the star particles. This leads to the enrichment of gas, which is otherwise assigned an initial metallicity of $7 \times 10^{-8}$ $Z_\odot$. For readers interested in further details, please refer to Pillepich et al. (2018a).

BH accretion in IllustrisTNG is modelled based on the Eddington-limited Bondi–Hoyle formalism. The Eddington limit and the bolometric luminosities of the accreting BHs are computed based on an assumed radiative efficiency of $\epsilon_r = 0.2$. IllustrisTNG implements a two-mode AGN feedback model. For high Eddington ratios, 'thermal feedback' is implemented wherein a fraction of the radiated luminosity is deposited to the neighbouring gas. For low Eddington ratios, feedback is in the form of kinetic energy that is injected on to the gas at irregular time intervals along a randomly chosen direction. Zinger et al. (2020) showed that thermal feedback tends to dominate the total energy injection in $M_* \lesssim 10^{10.5}$ $M_\odot$ galaxies, whereas the kinetic feedback becomes important at $M_* \gtrsim 10^{10.5}$ $M_\odot$. The latter is responsible for producing the population of massive red elliptical galaxies at $z \lesssim 2$ (Weinberger et al. 2017). However, in our study which focuses on lower mass galaxies at higher redshifts ($z \sim 4$–7), the kinetic feedback is subdominant. Additionally, it turns out that the gas accretion rates of our BHs at these redshifts are small enough that even thermal feedback does not have a strong impact on the galaxy stellar masses (see Section 3.1). Therefore, in our simulations, the modelling of AGN feedback is largely inconsequential to the assembly of the overmassive BHs. Readers interested in further details about the TNG feedback model may refer to Weinberger et al. (2017) (see also Kannan et al. 2017).

Our simulations cannot adequately capture the small-scale BH dynamics because the limited mass resolution prevents them from fully resolving the BH dynamical friction force. This is particularly true for the seed populations as the background DM particles are $\sim 10$ times more massive. To prevent the seeds from encountering spuriously large kicks by the massive DM particles, BHs are 're-positioned' to the nearest potential minimum within its 'neighbourhood' defined by 64 nearest neighbouring gas cells. The BHs are promptly merged when at least one of them is within the 'neighbour search radius' ($R_{\rm Hsml}$) of the other. Note that the resulting BH merger rates are inevitably overestimated compared to the actual event rates that may be detectable by facilities such as the Laser Interferometer Space Antenna or LISA (Amaro-Seoane et al. 2017). In Section 3.8, we account for the impact of potential delays on the BH merger rates as well as the $M_{\rm bh}$ versus $M_*$ relations at various redshifts.

### 2.3 Black hole seed models

The key novel feature of the BRAHMA simulations is the implementation of a comprehensive BH seeding model. The full BRAHMA suite of simulations is comprised of several runs that span a wide range of seeding prescriptions with seed masses ranging from $\sim 10^3$ to $10^6$ $M_\odot$. In this work, we primarily focus on those simulations that model $M_{\rm seed} = 1.5 \times 10^5$ $M_\odot$ (or $1 \times 10^5$ $M_\odot/h$) seeds formed via the direct collapse of gas. Our seeding criteria are motivated by conditions that are believed to be ideal for DCBH formation, namely pristine dense gas with low angular momentum wherein cooling to temperatures below $\lesssim 10^4$ K is suppressed by LW radiation and dynamical heating during halo mergers. To identify and seed BHs in these environments, we designed the following set of seeding criteria.

(i) *Dense and metal-poor gas mass criterion*: Seeds are placed in haloes that exceed a critical threshold of gas mass that is simultaneously dense ($> 0.13\,cm^{-3}$; i.e. the star formation threshold) and metal-poor ($Z < 10^{-4}\,Z_\odot$). The threshold is chosen to be 5 $M_{\rm seed}$.

(ii) *Lyman–Werner flux criterion*: When this criterion is applied, the dense and metal-poor gas mass is also required to be illuminated by an LW flux that exceeds the critical value $J_{\rm crit}$. Additionally, star formation is suppressed in seed-forming regions with supercritical fluxes. In this work, we assume a critical LW flux of 10 $J_{21}$. We consider relatively low $J_{\rm crit}$ compared to values ($\gtrsim 1000$ $J_{21}$) predicted by small scale radiation hydrodynamics simulations and one-zone chemistry models (Shang et al. 2010; Sugimura et al. 2014), as they have been shown to be too restrictive (Bhowmick et al. 2022a) to form BH seeds. As noted earlier, such low $J_{\rm crit}$ values may be viable for DCBH formation in environments where the gas is also dynamically heated during halo mergers. Note that in the absence of an explicit treatment of radiative transfer, we use a semi-empirical approach to compute the LW radiation as detailed in Section 2.1.2 of Bhowmick et al. (2022a).

(iii) *Gas spin criterion*: Seeds are placed in haloes where the net spin of the gas is smaller than the maximum threshold for the onset of Toomre instability, i.e.

$$\lambda = \frac{|\vec{J}_{\rm spin}|}{\sqrt{2} M_{\rm gas} R_{\rm vir} V_{\rm vir}} < \lambda_{\rm max}, \tag{1}$$

where $\vec{J}_{\rm spin}$ is the spin of gas which is expressed in dimensionless units as $\lambda$. $M_{\rm gas}$, $R_{\rm vir}$, and $V_{\rm vir}$ are the gas mass, virial radius, and circular velocity, respectively. $\lambda_{\rm max}$ is the Toomre instability threshold. This criterion was based on the stability analysis of pre-galactic discs and the collapse of unstable discs to form DCBHs, as done in Lodato & Natarajan (2006). It was subsequently implemented in Natarajan & Volonteri (2012) and DeGraf & Sijacki (2020). For further details underlying the implementation of this criterion, please refer to Section 2.1.1 of Bhowmick et al. (2022a).

(iv) *Halo environment criterion*: This criterion ensures that seeds are placed in haloes that have at least one neighbouring halo of comparable or higher mass within a distance of five times its virial radius. The choice of this distance is somewhat arbitrary, but it is small enough to ensure that the BHs are only forming in rich environments. We could make this distance smaller and make the criterion more restrictive, but as we shall see, our current choice already leads to an underprediction of the BH masses compared to the *JWST* results. Further details underlying the implementation of this criterion are described in Bhowmick et al. (2024a). We apply it to

emulate the impact of dynamical heating of gas that may occur during major mergers of haloes. This dynamical heating can contribute to the suppression of $H_2$ cooling, thereby potentially allowing DCBH formation under the relatively low critical LW flux of 10 $J_{21}$ assumed by us (Wise et al. 2019; Regan et al. 2020b, c). To that end, we note that our seed model is fully self-consistent only when both the *LW flux criterion* and the *halo environment criterion* are applied together. Nevertheless, we do run a simulation which only applies the *LW flux criterion* in order to isolate its individual impact and compare against that of the *halo environment criterion*.

Note also that in addition to the above, the DM mass resolution naturally imposes a minimum halo mass for seed formation. As we define a *resolved halo* to have at least 32 DM particles, seeds can only form in haloes above $7.1 \times 10^7$ $M_\odot$. Notably, this minimum value is close to the one suggested by Ferrara et al. (2014) for modelling $\sim 10^5$–$10^6$ $M_\odot$ DCBHs in cosmological simulations. Finally, all of the above seeding criteria were developed and tested within the AREPO code and the baseline TNG galaxy formation model using zoom simulations, over a series of prior papers (Bhowmick et al. 2021, 2022a, 2024a).

### 2.4 Simulation suite and nomenclature

Recall that we are using two different types of simulations based on whether they use unconstrained or constrained ICs. We run simulations with both ICs for each of our seed models.

To reasonably capture the impact of all the complex unresolved physics of DCBH formation in our simulations, we require all four seeding criteria described in the previous subsection. However, to test the importance of each criterion, we apply and stack them one at a time to produce four simulation boxes. The SM5 box solely applies the *dense and metal-poor gas mass criterion*. The SM5_LW10 box adds the *Lyman–Werner Flux criterion*. The SM5_LW10_LOWSPIN box additionally applies the *gas-spin criterion*. Finally, the SM5_LW10_LOWSPIN_RICH box includes all four criteria by also adding the *halo environment criterion*. In addition to the above simulations, we also show results from our predecessor IllustrisTNG simulations, particularly the highest resolution versions of the 100 Mpc (TNG100 with $1820^3$ DM particles) and 300 Mpc boxes (TNG300 with $2500^3$ DM particles).

## 3 RESULTS

### 3.1 High-redshift galaxy populations in BRAHMA

Since the stellar mass versus BH mass ($M_*$ versus $M_{\rm bh}$) relations can be influenced not only by the BH masses but also by their host galaxy stellar masses, it is instructive to first look at how our simulations compare with observations in terms of the galaxy populations. In Figs 1 and 2, we compare the UV LFs and galaxy stellar mass functions (GSMFs) between our unconstrained simulations and observations. The UV luminosities are computed from the global star formation rates of the galaxies as

$$M_{\rm UV} = -2.5 \log_{10} F_{\rm UV} - 48.6, \quad (2)$$

$$L_{\rm UV} = \log_{10}({\rm SFR}) + 28.1427, \quad (3)$$

where $M_{\rm UV}$, $F_{\rm UV}$, $L_{\rm UV}$, and SFR are the absolute UV magnitude, UV flux, intrinsic UV luminosity and the star formation rate, respectively, and the conversion from SFR to UV luminosity is taken from Madau & Dickinson (2014) assuming a Chabrier IMF. Despite the small volumes, our unconstrained boxes are able to probe a substantial portion of the observed galaxy populations, with UV magnitudes up to $M_{UV} \sim -20$ and galaxy stellar masses up to $\sim 10^{9.5}$ $M_\odot$ at $z \sim 5$. This is particularly encouraging as it has a significant overlap with the range of measured stellar masses of the *JWST* AGN hosts ($\sim 10^{7.5} - 10^{11}$ $M_\odot$). Recall that we use the constrained boxes to further extend the range of galaxy masses probed. This makes our simulations an ideal arena to study the typical BH populations that are expected to reside in these galaxies under various assumptions for BH seeding.

First, we note that the different BH seed models have no significant impact on the predicted UV LFs and GSMFs; this may be because the BH accretion rates are not large enough to induce significant AGN feedback on the host galaxies. In fact, we also find that the predictions between the unconstrained BRAHMA and TNG100 simulations (that seed BHs only based on halo mass) are very similar; this is not surprising as both TNG100 and BRAHMA use the same underlying galaxy formation model (except BH seeding). The BRAHMA and TNG100 UV LFs are broadly consistent with pre-*JWST* observational constraints at $M_{UV} \gtrsim -20$ (the measurements shown as black points in Fig. 1 are from the Hubble Frontier Field surveys). This is a testament of the remarkable success of the IllustrisTNG galaxy formation model as shown in Vogelsberger et al. (2020b) in this redshift range. At the bright end ($M_{UV} \lesssim -20$) that cannot be probed by the limited volume of BRAHMA, the overestimation of the TNG100 UV LFs is due to the absence of a correction for dust attenuation in our calculation of the $M_{\rm UV}$. Vogelsberger et al. (2020b) showed that with the inclusion of dust, the simulations also reproduce the bright end of the observed UV LFs.

Note that the negligible impact of AGN feedback on our simulated galaxies is somewhat distinct from the scenario considered by Pacucci & Loeb (2024) wherein AGN feedback is expected to substantially impact the host galaxies of the *JWST* BHs. As we shall see in Section 3.3, the BHs in our simulations grow largely via mergers. In this scenario, the presence of enough seeds can lead to substantial BH growth without impacting the host galaxy via AGN feedback. However, the Pacucci & Loeb (2024) model assumes that the *JWST* BHs accumulate their masses purely via accretion. In such a case, the required accretion rates would naturally be much higher than in our simulations, wherein we can expect a substantial impact of AGN feedback on the host galaxies.

The advent of *JWST* has now made it possible to also constrain the stellar mass functions at these redshifts (see Fig. 2). At $z \sim 4$ & 5, respectively, the simulated GSMFs show reasonable agreement with observations. At higher redshifts ($z \sim 6$ & 7), the simulations start to underpredict the abundances of $\gtrsim 10^8$ $M_\odot$ galaxies compared to the measurements. To that end, we note that the stellar masses are prone to be overestimated if the potential contributions from AGN are not accurately included. Additionally, we also know that at much higher redshifts ($z \gtrsim 10$), TNG follow-up projects such as THESAN (Kannan et al. 2022) and Millennium-TNG (Pakmor et al. 2023) also tend to underpredict the abundances of the galaxies observed by *JWST* (Kannan et al. 2023). Resolving these descrepancies would potentially require modifications to several aspects of our galaxy formation model such as star formation, metal enrichment and stellar feedback. This can also have substantial implications for BH seeding, which we shall explore in future work. For now, the fact that the IllustrisTNG galaxy formation model produces reasonable agreement between our simulations and *JWST* measurements at $z \sim 4$ and 5, means that at least at these redshifts, any differences in the intrinsic $M_*$ versus $M_{\rm bh}$ relations between the simulations and that inferred from observations, are likely to be much more readily attributable to the BH mass assembly rather than the galaxy stellar mass assembly.

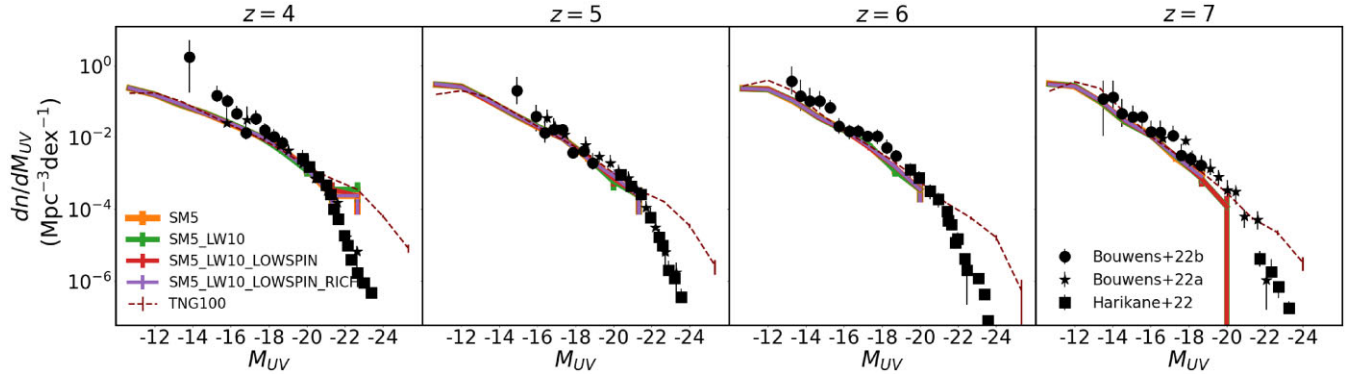


**Figure 1.** Galaxy UV LFs at $z = 4, 5, 6$ & 7 predicted by the unconstrained BRAHMA boxes, compared against measurements using Hubble Frontier Field observations (black data points) from Bouwens et al. (2022a), Harikane et al. (2022), and Bouwens et al. (2022b). The maroon dashed lines show predictions from TNG100. The BH seed models have no significant consequence on the UV LFs. The simulations and observations are broadly consistent with each other at $M_{\rm UV} \gtrsim -20$. At the bright end ($M_{\rm UV} \lesssim -20$), the absence of dust modelling causes TNG100 to overestimate the UV LFs.

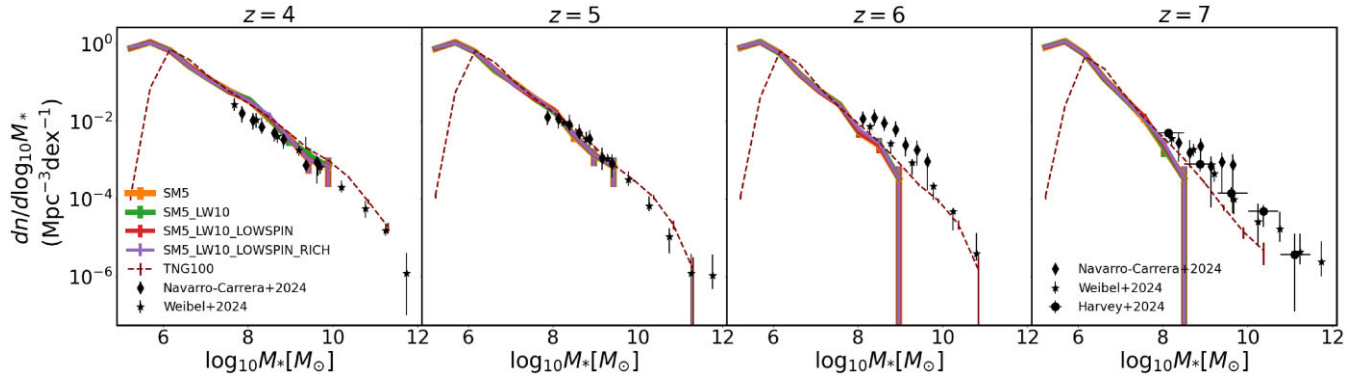


**Figure 2.** Galaxy stellar mass functions at $z = 4, 5, 6$ & 7 predicted by the unconstrained BRAHMA boxes, compared against recent measurements from *JWST* observations (black data points) from Navarro-Carrera et al. (2024) and Weibel et al. (2024). The maroon dashed lines show predictions from TNG100. The BH seed models have no significant consequence on the stellar mass functions. Both BRAHMA and TNG100 predictions are broadly consistent with the observations at $z \sim 4$ & 5, but the simulations tend to underpredict compared to the observations at $z \sim 6$ & 7.

### 3.2 Seed formation history

Having established that the simulated galaxy populations in the BRAHMA boxes are broadly consistent with observations, we now focus on the BH assembly under different seeding assumptions. We begin by looking at the seed formation history of the four simulation boxes shown in Fig. 3. For all the different seed models, the onset of seed formation occurs at $z \sim 25$ in both the constrained and unconstrained boxes. This coincides with the earliest collapse of gas to densities greater than the star formation threshold (hereafter referred to a 'dense gas') in a pristine universe. Continued onset of dense gas formation leads to a ramp-up of seed formation between $\sim 25 - 12$. However, the formation of stars and the resulting stellar feedback drives metal enrichment of gas, which eventually slows down seed formation. The peak of seed formation occurs at $z \sim 12$, after which their production is suppressed due to metal pollution. Notably, this is in broad agreement with the results of Yue et al. (2014) that uses an empirical model to find that DCBH formation peaks at $z \sim 13$. The slightly later peak formation time in our simulations may be because we use a smaller critical flux compared to the values (30–150 $J_{21}$) considered in their work. This follows from our earlier work (Bhowmick et al. 2022a, see fig. 8), wherein we found that higher critical LW fluxes shift the peak of seed formation to earlier times.

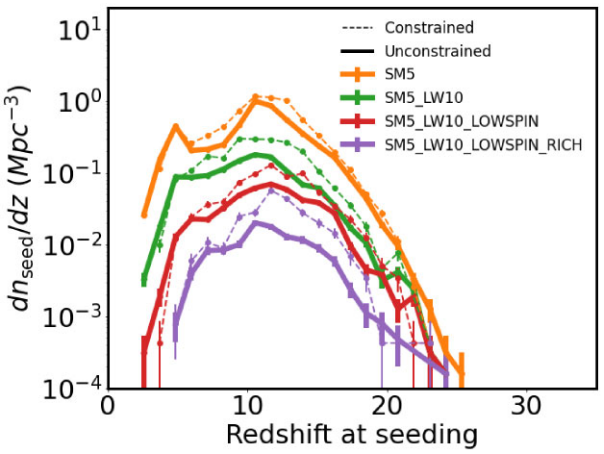


**Figure 3.** Distribution of seed formation redshifts for the four different seed models. The solid and dashed lines show the unconstrained and constrained simulations, respectively. As we stack up the different seeding criteria, the seed formation rates start to decrease. In the unconstrained simulations, at the peak of seed formation at $z \sim 12$, the most lenient SM5 seed model produces $\sim 1$ seed per Mpc$^3$, whereas the strictest SM5_LW10_LOWSPIN_RICH seed model produces $\sim 0.01$ seeds per Mpc$^3$.

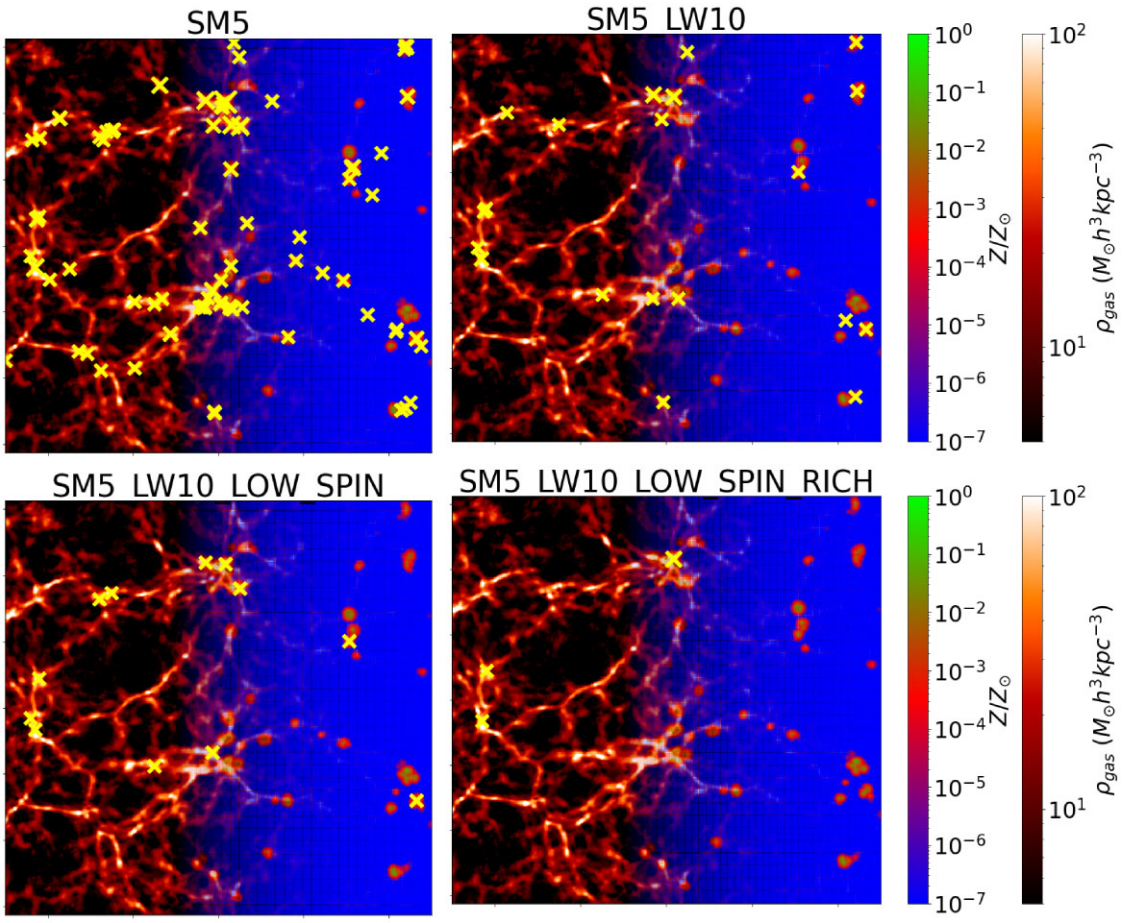


**Figure 4.** Visualization of the 18 Mpc unconstrained simulated boxes on a 50 kpc slice at $z = 5$, for the four different seed models. The left side of the panels show the projected gas density profiles, which smoothly transitions in to the projected gas metallicity profiles on the right side of the panels. The yellow crosses show the positions of BHs. For the most lenient SM5 seed model (top left), BHs occupy a significant majority of the regions with dense gas. However, for the strictest seed model SM5_LW10_LOWSPIN_RICH, only a small fraction of them host BHs.

Let us first look at the seed formation rates for the different models in the unconstrained simulations (solid lines in Fig. 3). For the most lenient SM5 model, the seed production peaks at $\sim 1$ seed per Mpc$^{-3}$ per unit redshift. For the remaining SM5_LW10, SM5_LW10_LOWSPIN, and SM5_LW10_LOWSPIN_RICH simulations, the peak seed production is reduced to $\sim 0.1$, $\sim 0.06$, and $\sim 0.01$ Mpc$^{-3}$ per unit redshift, respectively. The differences in seed formation rates tend to be larger at lower redshifts. This is because the impact of the gas-spin and Lyman–Werner flux criteria becomes stronger with decreasing redshift, as demonstrated in Bhowmick et al. (2022a). For the Lyman–Werner flux criterion, the greater suppression of seed production at later times is because of the reduction of the fluxes due to Hubble expansion. For the gas-spin criterion, this may be due to the gradual build-up of angular momentum of gas inside haloes as time evolves. These seed model variations have strong implications for the $z \sim 4 - 7$ BH populations, which can be readily seen in Fig. 4, which shows two-dimensional projection plots of the gas density and gas metallicity fields at $z = 5$. In the most lenient seed model SM5, BHs occupy a vast majority of the overdense regions. On the other hand, for the SM5_LW10_LOWSPIN_RICH model, only a tiny fraction of the overdense regions are occupied by BHs.

For the constrained simulations (dashed lines in Fig. 3), the seed model variations are qualitatively similar to the unconstrained simulations. However, for a given seed model, the constrained simulations do form larger numbers of seeds overall. For the SM5, SM5_LW10, and SM5_LW10_LOWSPIN simulations, the constrained boxes form $\sim 2$–3 times higher number of seeds compared to their unconstrained counterparts. But notably, when the halo environment criterion is applied, the impact of the constrained ICs is slightly stronger, with the constrained simulations producing $\sim 5$ times more seeds. This is not surprising given that the halo environment criterion favours seeding in rich environments, which are naturally more abundant within the constrained simulations. Fig. 5visualizes the constrained region, which clearly contains a strongly overdense peak close to the centre of the box. This is in stark contrast to the unconstrained region (top two rows) which contains relatively smaller overdensity peaks that are uniformly spread throughout the simulation volume. As a result, the BHs in the constrained simulations are much more strongly clustered than in the unconstrained simulations.

### 3.3 BH growth: mergers versus accretion

Having discussed the formation history of seeds, we now consider their subsequent growth to form higher mass BHs. In particular, we quantify the relative contributions of BH mergers and gas accretion to the overall BH mass as shown in Fig. 6. We show this for BH populations at snapshots $z = 7$ & 4 that bracket our redshift

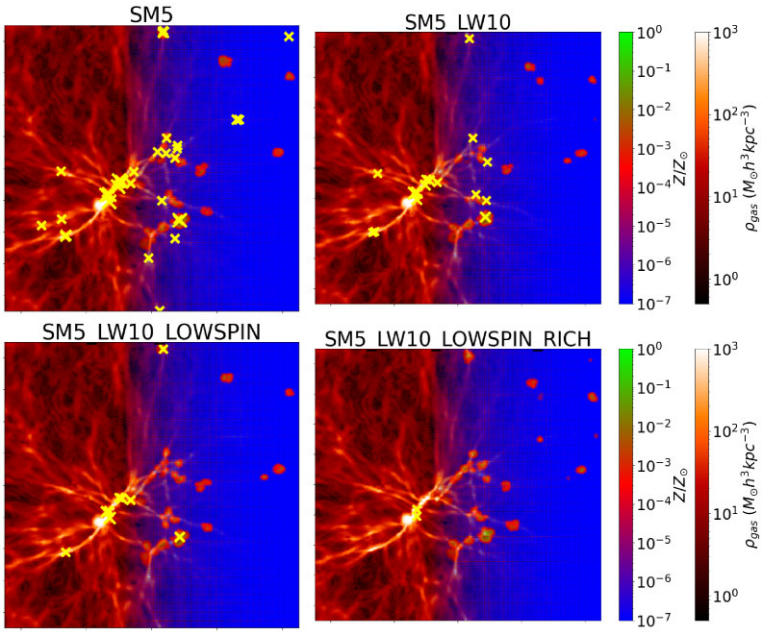


**Figure 5.** Similar to the previous figure, but for the 13 Mpc constrained simulation boxes on a 50 kpc slice at $z = 5$, for the four different seed models. We can see that the BHs are much more strongly clustered compared to the unconstrained boxes, leading to enhancements in merger rates.

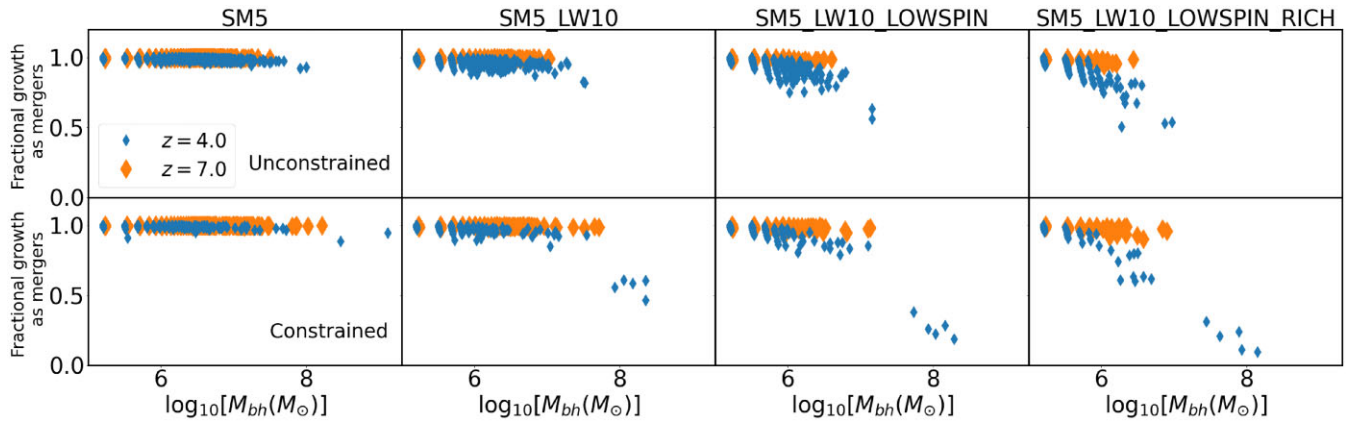


**Figure 6.** The fraction of the overall BH mass that is contributed by merger driven BH growth. The top and bottom panels show the unconstrained and constrained simulations, respectively. The orange and blue colours correspond to BHs at $z = 7$ and $z = 4$, respectively. BH growth is generally dominated by mergers. As we make the seed model more restrictive, the relative contribution from gas accretion increases, particularly for more massive BHs at lower redshifts.

range of interest. We can immediately see that in the unconstrained runs (top panels), the most massive BH formed by $z = 4$ with the most restrictive seed model (SM5_LW10_LOWSPIN_RICH) is only $\sim 10^7$ M$_\odot$, whereas the majority of the $z \sim 4 - 7$*JWST* BHs exceed that mass. This already hints that the combination of all the seeding criteria in Section 2.3 makes DCBH formation too restrictive to assemble the *JWST* BHs. In fact, the *JWST* BHs have masses up to $\sim 10^8$ M$_\odot$, which can only be achieved by the least restrictive seed model (SM5) in the unconstrained runs. The constrained runs (bottom panels) do produce higher mass BHs. However, as we shall see in Section 3.7, these BHs also live in higher mass galaxies. In other words, *at fixed* galaxy stellar mass, the constrained runs do not produce higher BH masses compared to the unconstrained runs.

We find that regardless of the seed model, the BH mass accumulation is dominated by mergers at $z = 7$ for both constrained and unconstrained simulations. We also saw this in our earlier works based on these seed models (Bhowmick et al. 2021, 2024a, b). In fact, for the most lenient seed model, the contribution from BH mergers continues to dominate ($\gtrsim 95$ per cent) even at $z = 4$. It is only when we make the seed models more restrictive that there is a natural reduction in merger driven growth that increases the relative importance of gas accretion. Only for the most massive $z = 4$ BHs formed by the most restrictive SM5_LW10_LOWSPIN_RICH seed model, the accretion-driven growth contributes $\sim 50$ per cent and $\sim 90$ per cent of the BH mass within the unconstrained and constrained simulations, respectively. Nevertheless, for the vast majority of BHs at these redshifts, the mass growth is pre-dominantly driven by BH mergers. This is contributed by two things: First, the $M_{\rm bh}^2$ scaling of our Bondi accretion formulae naturally leads to very low accretion rates in lower mass BHs, which makes it

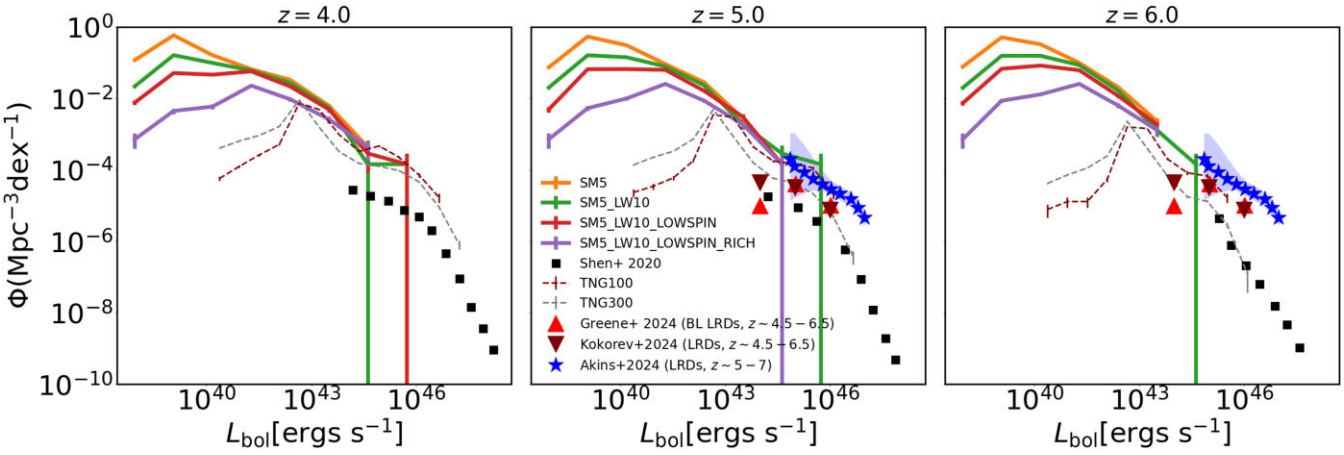


**Figure 7.** AGN bolometric LFs at $z \sim 4, 5$ & 6 for the four different BRAHMA boxes compared against observational constraints from pre-*JWST* quasars (Shen et al. 2020) as well as from the *JWST* LRDs measured by Kokorev et al. (2024) and Greene et al. 2024 (lower limits). The blue stars show the most recent measurements by Akins et al. (2024) using LRDs from the COSMOS-Web survey, under the assumption that all the LRDs are AGNs. These constraints are compared to the predictions from our unconstrained simulations. The maroon and grey dashed lines show the predictions from TNG100 and TNG300, respectively, that seed $10^6$ $M_\odot$ BHs based on a halo mass threshold of $7 \times 10^{10}$ $M_\odot$. The different seed models produce similar LFs at $\gtrsim 10^{43}$ erg s$^{-1}$.

difficult to grow them using gas accretion alone. Second, stellar feedback can significantly restrict the availability of enough gas to feed BHs, particularly in lower mass haloes at high redshifts wherein the potential wells are relatively shallow (Habouzit, Volonteri & Dubois 2017). In any case, one important implication of merger driven BH growth is that the build-up of higher mass BHs relies on the availability of sufficient seeds to undergo mergers. As a result, the choice of our seed model has a substantial impact on the final BH masses at $z \sim 4$–7 as mentioned in the previous paragraph. We shall discuss this further in Section 3.7, wherein it will be evident that the merger-dominated BH growth is very consequential to the feasibility of different seed models in producing $M_* - M_{\rm bh}$ relations that are consistent with those inferred from the measured *JWST* BHs.

### 3.4 AGN LFs

As we find that gas accretion has a negligible contribution to the BH growth in our simulations at these high redshifts, it is instructive to look at the AGN LFs and compare against available observational constraints. We start by looking at the bolometric LFs, since they can be most directly predicted by our simulations without any underlying assumptions about the AGN spectral energy distributions. In Fig. 7, we show the AGN bolometric LF predictions at $z = 4, 5$ & 6 for our different seed models as predicted by our unconstrained simulations. The BRAHMA boxes probe bolometric luminosities up to $\sim 10^{44}$ erg s$^{-1}$ before Poisson noise starts to dominate.[1,2] Before we focus on the comparison with observational constraints in the next paragraph, it is interesting to note here that the seed model variations are significant only for the faintest $L_{\rm bol} \lesssim 10^{41}$ erg s$^{-1}$ AGN. At $\gtrsim 10^{43}$ erg s$^{-1}$, the LFs are similar amongst the different BRAHMA seed models. The lack of seed model variations in the AGN LFs has also been shown in our previous papers for a wide range of seed models (Bhowmick et al. 2021, 2024b). To briefly summarize, we found that while the seed models produce differences in the overall number of BHs, the number of 'active' BHs remain similar as there are only a limited set of environments that provide enough gas to accrete and produce AGN at these high redshifts.[3] In fact, at $\gtrsim 10^{43}$ erg s$^{-1}$, the BRAHMA seed model predictions are also similar to TNG100 which simply seeds $10^6$ $M_\odot$ BHs when haloes exceed $7 \times 10^{10}$ $M_\odot$.[4] We also note that the TNG LFs sharply peak and fall off at luminosities below a few times $\sim 10^{42}$ erg s$^{-1}$. This is due to the higher seed mass ($10^6$ $M_\odot$) and the halo mass seeding threshold ($7 \times 10^{10}$ $M_\odot$) in TNG. This sharp fall off does not occur in our BRAHMA boxes in which there is a large number of $\lesssim 10^{42}$ erg s$^{-1}$ AGN that are fuelled by $\sim 10^5$–$10^6$ $M_\odot$ BHs residing in galaxies that are not massive enough to be seeded in TNG.

Due to the limited volume in our boxes, the overlap with observations is only at the brightest end of the simulation predictions ($\sim 10^{43}$–$10^{44}$ erg s$^{-1}$ at $z \sim 5$) wherein the seed model variations are very small. At this end, our predicted BRAHMA AGN LFs have a higher normalization than the pre-*JWST* observational constraints (black squares) from Shen et al. (2020) at $z \sim 4$ & 5. This is also the case for the TNG100 and TNG300 boxes which predict AGN LFs similar to our BRAHMA boxes despite having a very different seed model. As a result, the discrepancy with observations is unlikely to be originating from our seed models. In fact, a vast majority of simulations overpredict the AGN LFs compared to observational constraints at $z \sim 0$–4 (Habouzit et al. 2022). In

[1]While the constrained simulations do produce higher luminosities, they cannot be used to make volume independent AGN LF predictions as their IC realizations are not a representation of an average volume.

[2]The brightest AGN produced by the different boxes at a given snapshot can vary between $\sim 10^{44}$ and $10^{46}$ erg s$^{-1}$. However, these variations are simply due to the large time-variability of the AGN luminosities, and not necessarily due to the seed models.

[3]Note that despite the merger dominated BH growth at $z \gtrsim 3$, we also showed in Bhowmick et al. (2024b) that BH mass assembly due to gas accretion starts to become comparable to mergers at $z \lesssim 3$. Gas accretion eventually dominates the BH mass assembly at $z \sim 0$, consistent with the Soltan argument.

[4]Despite having the same physics, TNG300 and TNG100 AGN LFs differ by factor of 3–5, due to the different simulation resolutions. TNG300 produces lower luminosities likely because it cannot resolve the high density peaks as effectively as TNG100.

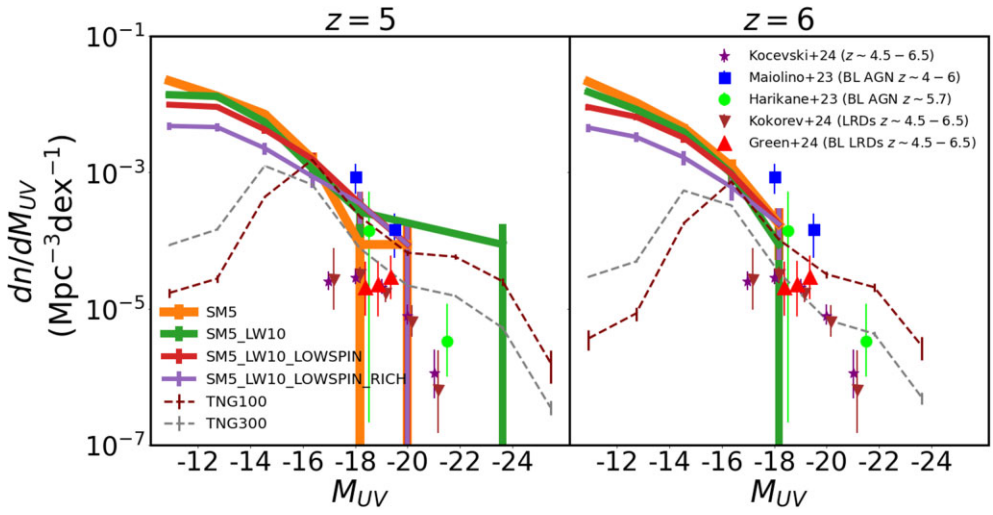


**Figure 8.** AGN UV LFs at $z \sim 5$ & 6 for the four different BRAHMA boxes compared against observational constraints from *JWST* AGNs. Here, we show predictions from the unconstrained simulations. For the UV luminosities, the bolometric corrections were adopted from Shen et al. (2020). There is a significant spread in the observed measurements, but the simulation predictions are broadly consistent with them.

the future, we will investigate other aspects of the BH physics modelling (such as BH accretion and dynamics) to explore the reasons for this discrepancy. At the same time, the discrepancy can also be due to uncertainties in the observational measurements within the modelling of AGN obscuration as well as bolometric corrections. This is hinted within the recent constraints from *JWST* AGN that are lower limits (red triangles in Fig. 7) at $z \sim 5$ derived by Greene et al. (2024) as well as constraints from Kokorev et al. (2024). We can see that these *JWST* based measurements are slightly higher than the pre-*JWST* measurements from Shen et al. (2020), bringing them closer to the simulations. Notably, the very recent measurements by Akins et al. (2024) used LRDs from the COSMOS-Web survey (blue stars in Fig. 7) and inferred a slightly even higher LF compared to Greene et al. (2024) and Kokorev et al. (2024). These measurements are also broadly consistent with the simulations at $\sim 10^{44}$ erg s$^{-1}$, while being $\sim 100$ times higher than the pre-*JWST* quasars at the most luminous end ($\gtrsim 10^{46}$ erg s$^{-1}$) that is too rare for our simulations to probe. However, the Akins et al. (2024) measurements are likely to be upper-limits, as they were explicitly made under the assumption that *all* the LRDs are AGN dominated.

While very few measurements of the bolometric AGN LFs have been made due to the uncertainty in the bolometric corrections, there are several measurements in the rest frame UV band. Given the greater availability of UV LF measurements, it is worthwhile to compare them against our simulations even though the conversion of the simulated bolometric luminosities to UV luminosities will carry similar bolometric correction uncertainties. Therefore, in Fig. 8, we convert the simulated bolometric LFs to rest frame UV LFs using the bolometric correction from Shen et al. (2020). We compare the $z = 5$ & 6 snapshot predictions to the *JWST* measurements for $z \sim 4.5$–6.5 AGN samples. Here again, the overlap between simulated and observed regimes is only over a very small range of $M_{\rm UV} \sim -17$ to $-20$. There is also a significant spread amongst the observational constraints. However, it is still noteworthy that our simulations predict broadly consistent AGN abundances between $M_{UV} \sim -17$ and $-20$ that are well within the range of current observational measurements.

As future *JWST* observations lead to more precise constraints, it will shed further light on whether or not our simulations predict AGN LFs that are consistent with observations at these redshifts. Nevertheless, one clear outcome from this analysis is that despite our BRAHMA simulations exhibiting merger dominated BH growth at these redshifts, the predicted AGN activity is not substantially smaller than what is inferred from observations.

### 3.5 AGN–galaxy connection

Based on the galaxy stellar mass functions and AGN LFs, it is clear that the number densities ($\sim 10^{-2}$ Mpc$^{-3}$) of typical galaxies with the measured stellar masses of *JWST* AGN hosts ($\gtrsim 10^{7.5}$ M$_\odot$) are much larger than the inferred number densities of the AGNs themselves (ranging from $\sim 10^{-5}$ *to* $10^{-3}$ Mpc$^{-3}$). This could suggest that the *JWST* AGNs are observed at luminosities much higher than the typical population of BHs living in these galaxies. Given that our simulations are able to broadly reproduce the abundances of both galaxies and AGNs, it is instructive to also look at the simulations and the *JWST* observations on the stellar mass versus AGN luminosity ($M_*$ versus $L_{\rm bol}$) plane.

Fig. 9 shows the $M_*$ versus $L_{\rm bol}$ relations for the simulations, plotted with observations from Harikane et al. (2023). The simulations show a clear positive correlation between $M_*$ and $L_{\rm bol}$. For the BRAHMA boxes, we only show results for the most lenient (SM5) and the most restrictive (SM5_LW10_LOWSPIN_RICH) seed models for clarity. Note that both these seed models produce broadly similar results that are also similar to the TNG300 predictions (except for the faintest $\lesssim 10^{42}$ erg s$^{-1}$ AGNs living in the smallest galaxies). This shows that our seed models do not substantially impact the $M_*$ versus $L_{\rm bol}$ relations, which is expected given the earlier results from Figs 7 and 8 that showed that AGN LFs are also not significantly sensitive to the seed model (except the faintest end $\lesssim 10^{41}$ erg s$^{-1}$).

Let us now focus on the comparison with observations. The Harikane et al. (2023) sample contains several $\gtrsim 10^{44}$ erg s$^{-1}$ AGN living in $M_* \gtrsim 10^8$ M$_\odot$ galaxies. However, in our simulations, the typical AGN luminosities in $M_* \sim 10^8$ M$_\odot$ galaxies are a few times

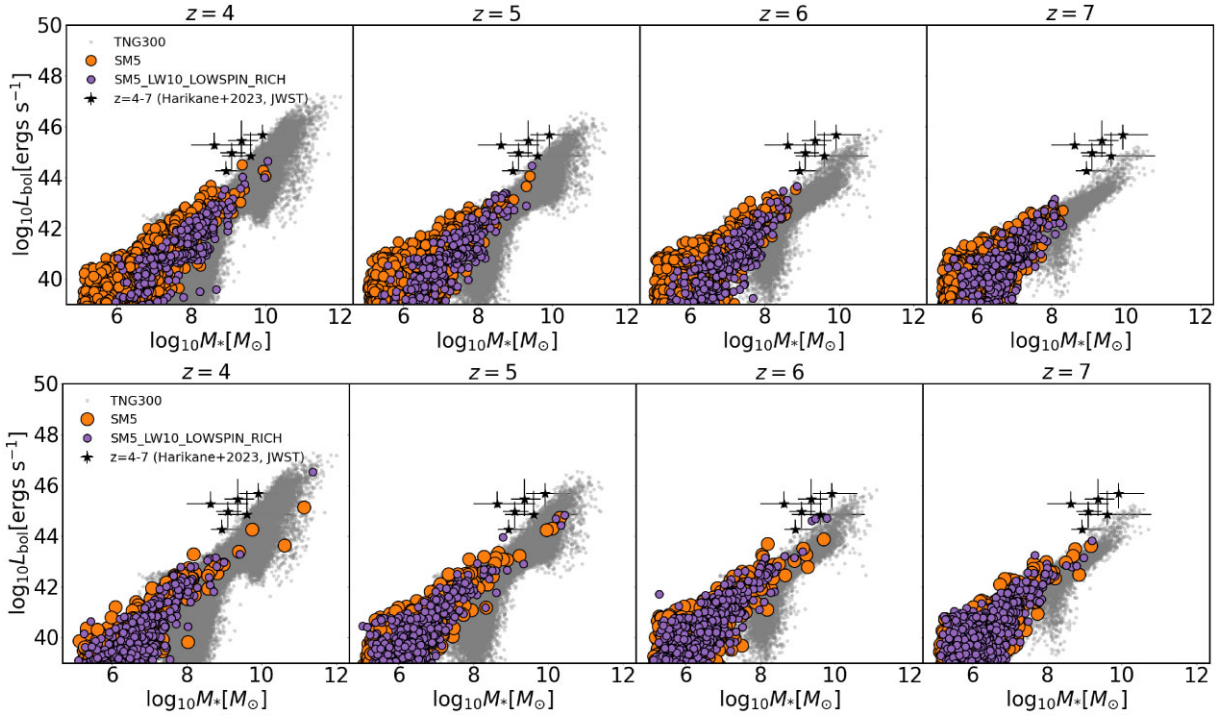


**Figure 9.** Stellar mass versus AGN bolometric luminosity relations ($M_*$ versus $L_{\rm bol}$) at $z = 4$, 5, 6 & 7 produced by our simulations compared against the *JWST* observations at $z \sim 4-7$. The top and bottom panels correspond to the constrained and unconstrained simulations, respectively. At the observed luminosities, the simulated AGN host galaxies have higher stellar masses compared to observed measurements.

$\sim 10^{42}$ erg s$^{-1}$ at $z = 4$ & 5. In a similar vein, the simulated AGNs with $\gtrsim 10^{44}$ erg s$^{-1}$ typically only live in $M_* \gtrsim 10^9$ M$_\odot$ galaxies i.e. $\sim 10$ times higher than the measurements for the *JWST* AGN hosts. This discrepancy in the simulated and observed $M_*$ versus $L_{\rm bol}$ relations is not surprising given that the AGN LFs are broadly consistent between them. This is because, given that the galaxy abundances are much higher than the AGNs, if the simulated $M_*$ versus $L_{\rm bol}$ relations were actually consistent with observations, the simulations would have dramatically overpredicted the AGN LFs.

As mentioned in the introduction, it is possible that *JWST* is only observing AGNs significantly above the intrinsic $M_*$ versus $L_{\rm bol}$ relation due to Lauer bias. While the scatter in the BRAHMA $M_*$ versus $L_{\rm bol}$ relations is not large enough to produce any up-scattered $\sim 10^{44}$ erg s$^{-1}$ AGN in $\sim 10^8$ M$_\odot$ galaxies, we acknowledge that this may be simply due to the limited volume of the BRAHMA boxes. However, we can also clearly see that even the TNG300 simulation (see grey points in Fig. 9) that has a volume much larger than the *JWST* fields, does not produce any up-scattered AGNs that overlap with the observations. This firmly establishes that our galaxy formation model can only produce the observed AGN luminosities in galaxies with stellar masses significantly higher than the measurements for the *JWST* AGNs.

The above analysis implies that if the discrepancy in the $M_*$ versus $L_{\rm bol}$ relations is solely due to Lauer bias, then the scatter in $M_*$ versus $L_{\rm bol}$ relations in the high-$z$ Universe must be substantially higher than what our simulations predict. As more luminous AGNs tend to be powered by more massive BHs, the BH masses will also be impacted by Lauer bias (which we address in the next section). However, in addition to Lauer bias, there could be contributions from other possible sources to this discrepancy that would impact the observed luminosities without necessarily impacting the observed BH masses. First, there may be Eddington bias due to rapid variability in the AGN luminosities since the detection likelihood would be much higher during the peak luminosities. This would lead to observed luminosities being significantly higher than the actual time-averaged luminosities (if they are below observational limits). Notably, this possibility has been explored in the galaxy sector i.e. to explain the excess of highest-$z$ ($z \gtrsim 9$) *JWST* galaxies compared to theoretical predictions as a consequence of UV variability from bursty star formation (Shen et al. 2023). It is also well-known that AGN variability has an inverse scaling relation with BH mass (Ponti et al. 2012; Kelly et al. 2013), making these *JWST* AGNs more susceptible to Eddington bias compared to the pre-*JWST* quasars. Secondly, the stellar masses of the AGN hosts may be underestimated as it is often difficult to separate the contribution from the AGN and the host galaxy within the observed light (Ramos Padilla et al. 2020). It is also important to note that while the current BH masses are also highly uncertain and are prone to systematic biases, the discrepancy in the simulated and observed $M_*$ versus $L_{\rm bol}$ relations is independent of the BH mass measurements. It will be interesting to revisit this discrepancy in future work as we anticipate the continued detection of new high-$z$ AGNs and more precise stellar mass estimates. For now, it is nevertheless encouraging to see that the simulations are in broad agreement with both the galaxy stellar mass functions and AGN LFs. For the remainder of the paper, we shall focus on the BH mass assembly, which is predominantly driven by mergers (as shown in Section 3.3).

### 3.6 Black hole merger rates

In Fig. 10, we show the rates at which BHs merge within our four different simulations. These mergers are expected to produce gravitational waves detectable with LISA. However, due to our

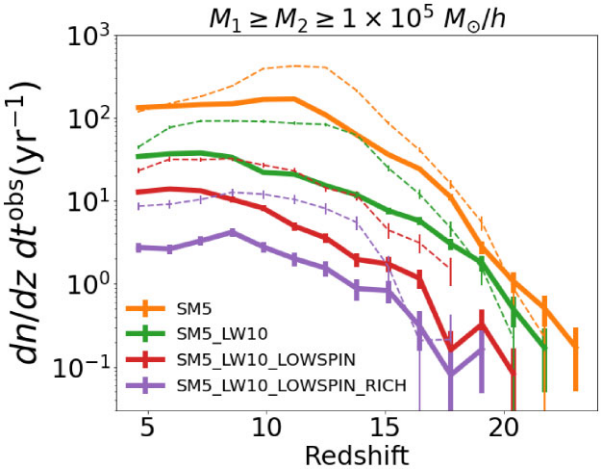


**Figure 10.** Predicted merger rates of BH binaries in our different simulation boxes with different seed models. This is defined to be the number of mergers ($dn$) that occur within a comoving shell from $z$ to $z + dz$, the signal for which will reach an observer on Earth within a time interval $dt_{\rm obs}$. The solid lines correspond to the unconstrained simulations and the dashed lines show the constrained simulations. The merger rates are strongly sensitive to the seed model. The unconstrained simulations produce peak merger rates of $\sim 200$ per year at $z \sim 12$ for our most optimistic seed model, and $\sim 4$ per year at $z \sim 9$ for the strictest seed model. Note that due to BH repositioning, these merger rates should only be interpreted as upper limits for the *true* merger rates detectable by LISA.

BH repositioning scheme, we are implicitly assuming the most optimistic scenario wherein for every galaxy merger, the BHs merge instantaneously. In reality, we expect these mergers to occur after a finite binary inspiral time, which could be a significant fraction of the Hubble time in some cases; this would depend on the eccentricities of the orbiting binaries as well as the effectiveness of processes that contribute to the hardening of the binaries at sub-kpc scales such as stellar loss-cone scattering, and drag due to circumbinary discs (Kelley, Blecha & Hernquist 2017; Sayeb et al. 2021; Siwek, Weinberger & Hernquist 2023; Siwek, Kelley & Hernquist 2024). Merger remnants can also get kicked out of the galaxies due to gravitational recoil (Blecha & Loeb 2008; Holley-Bockelmann et al. 2008; Volonteri & Madau 2008; Blecha et al. 2016; Gerosa & Moore 2016; Dunn, Holley-Bockelmann & Bellovary 2020), which can impact future mergers. Due to all these reasons, the results from Fig. 10 should only be interpreted as upper limits. Not surprisingly, we can see that the BH merger rates are strongly dependent on the seed model. For the unconstrained simulations, the most optimistic `SM5` model predicts peak merger rates of $\sim 200$ per year. The remaining `SM5_LW10`, `SM5_LW10_LOWSPIN` and `SM5_LW10_LOWSPIN_RICH` predict peak merger rates of 30, 10, and 4 per year, respectively. The constrained simulations generally predict $\sim 5$ times higher merger rates compared to their unconstrained counterparts for all seed models (solid versus dashed lines in Fig. 10). Notably, the constrained ICs enhance the merger rates more strongly than they enhance the seeding rates (revisit solid versus dashed lines in Fig. 3). This is because the BHs in the constrained ICs are much more clustered, allowing them to merge more efficiently compared to the unconstrained ICs.

Finally, as the BH growth is dominated by mergers at $z \gtrsim 4$, the differences in the merger rates for the different seed models have strong implications for the final BH masses accumulated at different redshifts, which we study in detail in the next section.

### 3.7 Stellar mass versus black hole mass relations: comparison with *JWST* observations

We finally look at the $M_*$ versus $M_{\rm bh}$ relation plotted in Figs 11 (unconstrained) and 12 (constrained) and compare them against the estimates based on *JWST* observations. However, we must be wary of the fact that (1) the existing BH mass measurements are highly uncertain (in addition to the stellar mass measurements as discussed earlier) and (2) the observed BHs are expected to be above the *intrinsic* $M_*$ versus $M_{\rm bh}$ relations due to Lauer bias and Eddington bias. If the bias is substantial, a direct comparison between the *JWST* measurements (shown as black points) and our complete sample of simulated BH populations would not be even-handed. As mentioned in the introduction, Pacucci et al. (2023) used a Markov Chain Monte Carlo (MCMC) approach to estimate the intrinsic $M_*$ versus $M_{\rm bh}$ relations (parametrized by a power law) using combined data from Harikane et al. (2023), Maiolino et al. (2023), Finkelstein et al. (2023), and Übler et al. (2023). Notably, the data only included those BHs that are spectroscopically confirmed with NIRSpec, and their black hole masses are estimated with the H $\alpha$ line (Greene & Ho 2005). Based on the measurements and H $\alpha$ FWHM detection limits, Pacucci et al. (2023) accounted for the Lauer bias and inferred a high-$z$ intrinsic $M_*$ versus $M_{\rm bh}$ relation (shown as solid black lines in Figs 11 and 12) that is still higher than the local relations by $> 3\sigma$. This relation (hereafter P23 relation) may be directly compared to our simulation predictions. Recall also that Li et al. (2024) used a similar approach (but using the flux limits instead of the H $\alpha$ FWHM limits) to infer a mean high-$z M_*$ versus $M_{\rm bh}$ relation that is consistent with the local BHs. However, they also infer a scatter that is $\sim 2$ times higher than that of the local relations. While it is not firmly established whether high-$z$ BHs indeed are systematically overmassive, it is a crucial time to use our simulations to explore implications of possible 'overmassive-ness' on the feasibility of different seed models.

We start by noting that even though the constrained simulations probe a much rarer overdense region and produce higher numbers of galaxies and BHs, their $M_*$ versus $M_{\rm bh}$ relations are very similar to the unconstrained simulations. This implies that the volume limitations in our simulations do not significantly impact the $M_*$ versus $M_{\rm bh}$ predictions. This enables us to robustly probe the impact of seed models on the $M_*$ versus $M_{\rm bh}$ relations. As clearly seen in Figs 11 and 12, the merger dominated BH growth in our simulations leads to the final BH masses (at fixed stellar mass) being substantially impacted by the seed model. More specifically, we find that as the seed models become more restrictive, our simulations produce smaller BH masses at fixed stellar mass. We also note that for a given seed model, as we go from $z = 7$ to $z = 4$, the $M_*$ versus $M_{\rm bh}$ relations shift rightwards as galaxy growth is faster than BH growth at these redshifts. As these observed samples continue to grow in the future, we shall hopefully be able to infer their redshift evolution and compare with our predictions. But for now, since most of the AGNs comprising the $z \sim 4$–7 composite P23 sample are actually at $z \sim 4$–5, we shall mostly focus on comparing these results with our $z = 4$ & 5 snapshot predictions.

For the most optimistic seed model (`SM5`: the first row of Figs 11 and 12) that produces the highest number of seeds, the BH masses are about $\sim 100$ times larger than implied by the local scaling relations (black dashed line). In $\sim 10^8$–$10^9$ $\rm M_\odot$ galaxies, this seed model produces BH populations that readily overlap with the *JWST* BHs on the $M_*$–$M_{\rm bh}$ plane at $z = 4$ & 5. When we include the LW flux criterion in `SM5_LW10` model, the resulting $M_*$ versus $M_{\rm bh}$ relations shift downwards, but continue to have some overlap with the *JWST* BHs. When we further add the gas spin and the halo environment

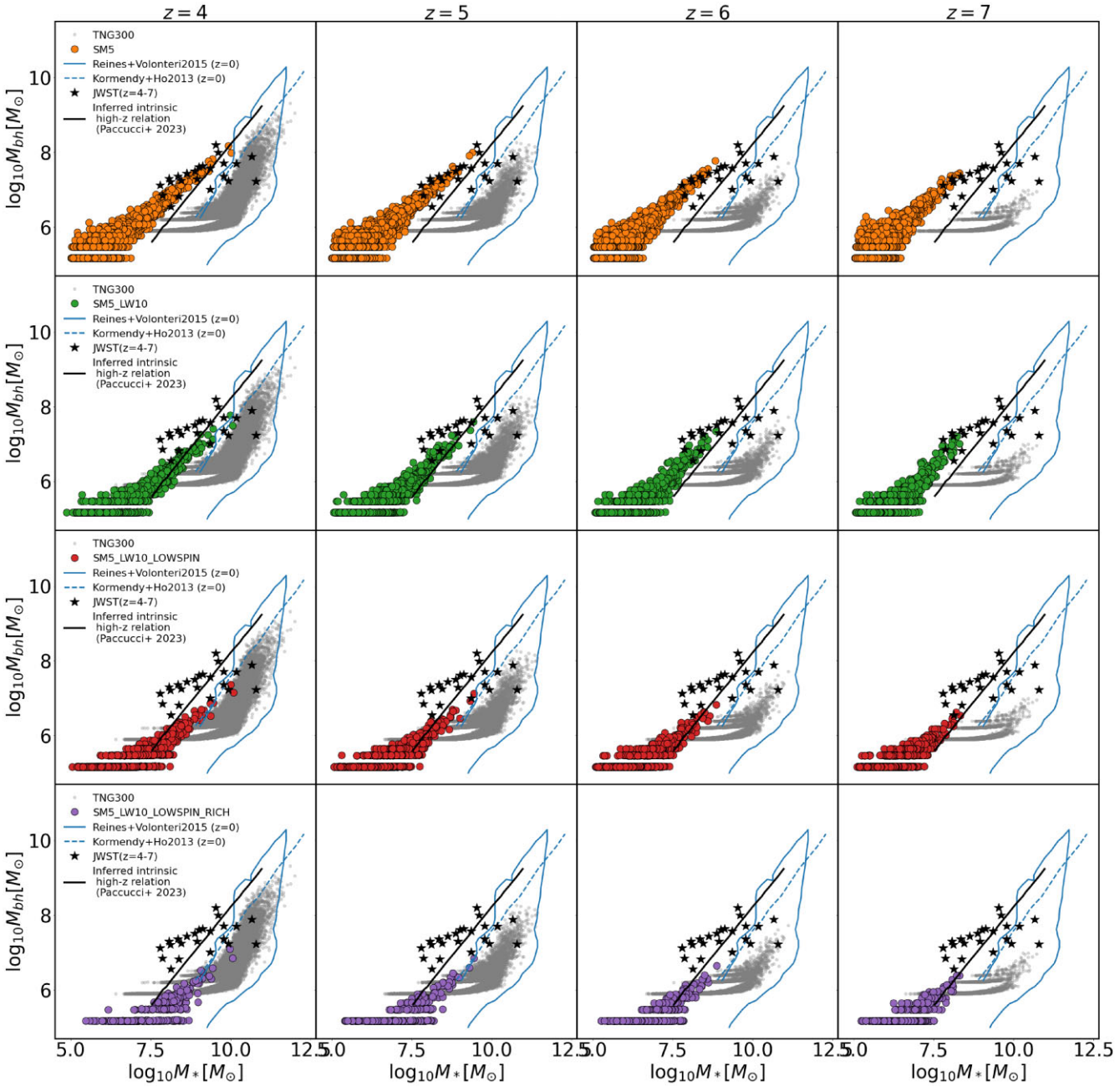


**Figure 11.** Stellar mass versus BH mass ($M_* - M_{\rm bh}$) relation predictions from our unconstrained simulations with different seed models (coloured circles). The solid black line shows the inferred intrinsic high-z relations inferred by Pacucci et al. (2023) based on *JWST* measurements from several works prior to it (black stars). These measurements have uncertainties (not shown for clarity) around $\sim$ 1 dex for both stellar and BH masses. The grey solid line approximately represents the scatter in local $M_*$–$M_{\rm bh}$ relation from Reines & Volonteri (2015). The grey dashed and dotted lines are the local measurements from Kormendy & Ho (2013) and Terrazas et al. (2016), respectively. At $z \sim$ 4–7, the most lenient seed model (SM5) has a substantial overlap with the *JWST* BHs. However, the most restrictive seed model that applies all the seeding criteria required for DCBHs significantly underpredicts the BH masses compared to the *JWST* BHs.

criteria (SM5_LW10_LOWSPIN and SM5_LW10_LOWSPIN_RICH), the resulting BH populations are significantly below the *JWST* BHs particularly within $M_* \lesssim 10^9$ M$_\odot$ galaxies. However, if these *JWST* measurements are subject to Lauer bias and are indeed up-scattered, comparing them to the full BH populations in our simulations would not be fair. Additionally, even if the underlying scatter in the $M_*$ versus $M_{\rm bh}$ relation is significant, our small simulation boxes will not capture BHs that are substantially up-scattered. Here again (as we did earlier for the $M_*$ versus $L_{\rm bol}$ relations), we can use the much larger TNG300 simulations to evaluate how much scatter we can expect if our seed models were applied to much larger volumes.[5] For the majority of the range of galaxy masses

[5]We caution however that the scatter in the $M_*$ versus $M_{\rm bh}$ relations produced in our seed models may be very different from the TNG seed model.

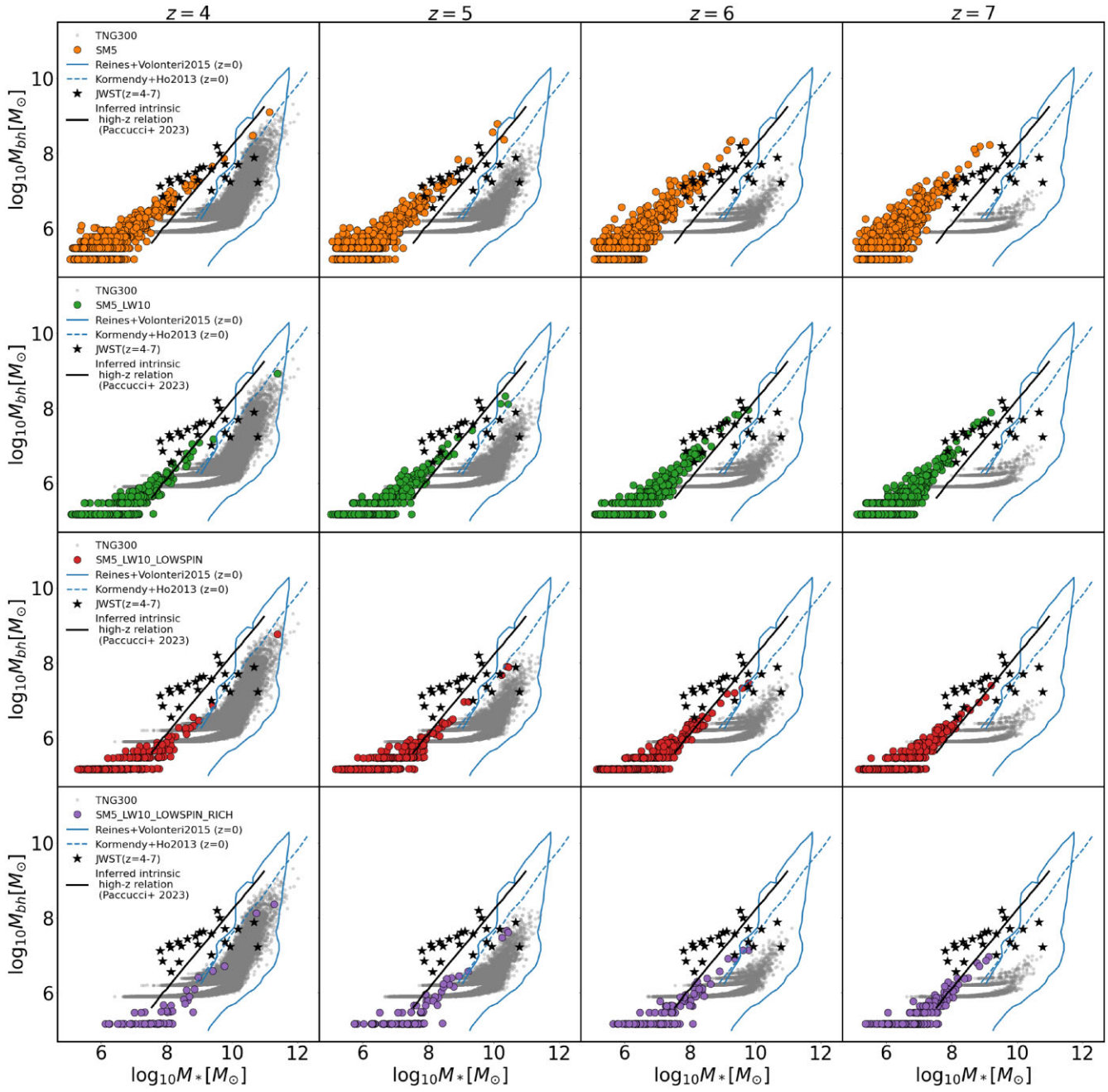


**Figure 12.** Similar to Fig. 11, but for the constrained simulations. For a given seed model, the $M_*$–$M_{\rm bh}$ relations are similar between the constrained and unconstrained runs. But the constrained runs are able to produce higher mass galaxies, fully covering the range of *JWST* host galaxy stellar masses at $z = 4$ & 5.

captured by TNG300, the scatter is roughly $\sim$ 1.5 dex.[6] Note that our most restrictive SM5_LW10_LOWSPIN_RICH seed model predicts a mean relation $\sim$ 1 dex below the *JWST* observations. For this model, if we assume a scatter of $\sim$ 1.5 dex, it would be difficult to produce BHs up-scattered enough to overlap with the *JWST* BHs even in a TNG300-like volume. We should also note that the *JWST* fields are substantially smaller than TNG300. All this suggests that assuming a $\sim$ 1.5 dex scatter, the mean $M_*$ versus $M_{\rm bh}$ relation predicted by SM5_LW10_LOWSPIN_RICH would imply a very small likelihood of *JWST* surveys containing these observed overmassive BHs. Therefore, even if we account for Lauer bias, SM5_LW10_LOWSPIN_RICH likely underpredicts the BH growth compared to what is required to produce the *JWST* measurements. At the other end, the most optimistic SM5 seed model already produces a mean $M_*$ versus $M_{\rm bh}$ relation that is overlapping with the presumably up-scattered *JWST* observations; this implies that in the event of significant Lauer bias, this model overpredicts the BH growth compared to what is inferred from *JWST* measurements.

[6]the $M_*$ versus $M_{\rm bh}$ relations in TNG300 flattens at $M_* \lesssim 10^9$ M$_\odot$ as a consequence of its underlying seed model ($\sim 10^6$ M$_\odot$ BHs seeded in halos above $\gtrsim 10^{10}$ M$_\odot$ haloes).

We must also bear in mind that if the scatter in the $M_*$ versus $M_{\rm bh}$ (and the $M_*$ versus $L_{\rm bol}$) relations were large enough, one could have a significant likelihood of detecting these *JWST* AGNs regardless of the location of the *mean* relation. Therefore, the possible confirmation of these *JWST* measurements could also imply that the scatter in these relations at high-$z$ is substantially larger than our simulation predictions. Recall that we reached similar conclusions for the scatter in the $M_*$ versus $L_{\rm bol}$ relations in Section3.5.

To summarize the above arguments, assuming that the high-$z$ scatter in the $M_*$ versus $M_{\rm bh}$ relations is not much larger than the TNG300 prediction of $\sim 1.5$ dex, our most restrictive SM5_LW10_LOWSPIN_RICH seed model likely underpredicts the BH growth whereas our most optimistic SM5 seed model likely overpredicts the BH growth. We shall now see how the foregoing is consistent with an 'apples-to-apples' comparison of our simulation predictions with the intrinsic P23 relation. The SM5 model predictions are higher than the P23 relations at $z = 4$ & 5. This indeed implies that the model produces too many seeds which merge with one another to produce $z \sim 4$–5 BH populations that are too massive. This is not unexpected as SM5 assumes that a heavy $\sim 10^5$ M$_\odot$ DCBH seed is produced in any region with sufficient dense and metal poor gas; this is unlikely to happen in most environments where the cooling due to molecular hydrogen will fragment the gas and prevent DCBH formation. When we include the LW flux criterion in the SM5_LW10 model, the resulting relations are very close to the P23 relation at $z = 4$ & 5 (particularly at $z = 4$). However, when we also include the gas spin and halo environment criteria (SM5_LW10_LOWSPIN and SM5_LW10_LOWSPIN_RICH), the $M_*$ versus $M_{\rm bh}$ relations shift further downward. The most restrictive SM5_LW10_LOWSPIN_RICH model substantially underpredicts the BH masses compared to the P23 relation by factors of $\sim 10$. Finally, the TNG300 simulation shows the maximum disagreement with the P23 relation as the simulated BHs are already at the local scaling relations by $z \sim 7$.

Overall, we find that when all the potential preconditions for DCBH formation are included in our seed model, the simulated $M_*$ versus $M_{\rm bh}$ relations are no longer consistent with what is inferred from the *JWST* observations. Recall that with our BH repositioning scheme, we are already assuming the most optimistic scenario for the merging efficiency of BH binaries. Therefore, our results suggest that in order to produce sufficiently overmassive BHs (as suggested by P23) using merger driven BH growth, we need additional heavy seeding channels compared to the standard DCBH scenario. These additional channels need to either form heavy seeds in higher numbers, or seeds that are much more massive than our assumption of $\sim 10^5$ M$_\odot$. The presence of light seeds can also boost the merger driven BH growth by merging with heavy seeds. Alternatively, one can also boost the BH growth due to gas accretion by allowing for accretion rates higher those inferred from the standard Bondi–Hoyle accretion formula, as recently explored in Jeon et al. (2024). Although not shown in any figures, we re-ran our most restrictive seed model with a Bondi boost factor of 100, as well as a reduced radiative efficiency of 0.1, but they only make a small difference to the final BH masses (up to factors of $\sim 2$) that are inconsequential to our main conclusions. This may be contributed by the difficulty in growing low mass BHs due to the $M_{bh}^2$ scaling of the Bondi accretion rate. In the future we plan to explore other accretion models beyond the Bondi–Hoyle model (that scale differently with BH mass), and also explore other aspects of our galaxy formation model that can influence the BH accretion rates (e.g. stellar feedback).

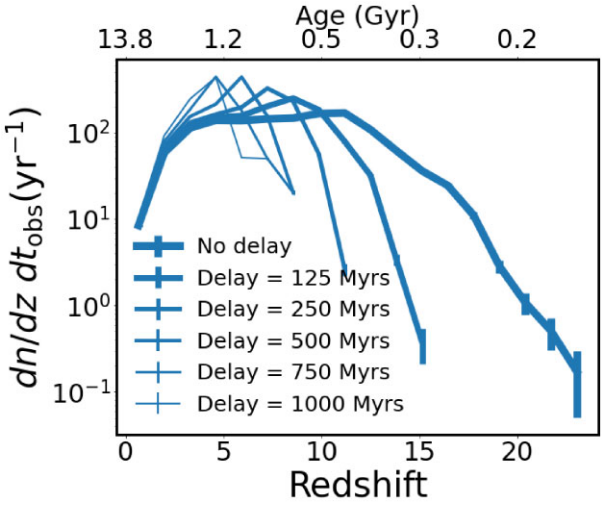


**Figure 13.** Predicted merger rates for the SM5 model under different assumptions for the delay times for the *true merger* (compared to the simulated merger). These are shown for the unconstrained simulations. As we increase the delay times, the merger rates are strongly suppressed at the highest redshifts, and the peak of the distribution occurs at lower redshifts.

### 3.8 Impact of delayed BH mergers

In the previous subsection, we found that only our most optimistic seed models (SM5 and SM5_LW10) produce BH populations that are broadly comparable to the *JWST* measurements as they currently stand. Additionally, the SM5 model overpredicts the P23 intrinsic high-$zM_*$ versus $M_{\rm bh}$ relation, while the SM5_LW10 is comparable to the P23 relation at $z = 4$ & 5. However, even for these models, the merger driven growth in BH mass is likely overestimated as our repositioning scheme promptly merges the BHs soon after their host galaxies merge. Additionally, prompt mergers could also overestimate merger rate predictions for LISA. In this section, we study the implications of a possible time delay between the BH mergers and galaxy mergers. We consider a simple model that assumes a uniform time delay ($\tau$), and reconstruct the merger histories of all the BHs at a given snapshot. In Fig. 13, we consider delay times of $\tau = 125, 250, 500, 750$ & 1000 Myr, and show the resulting merger rates for the SM5 model in the unconstrained simulations. Of course in reality, the delay times are not expected to be fixed and will likely scale with the dynamical time of the host halo. But due to the limited snapshot resolution, we are unable to track the host halos of all the BH mergers at the exact time they merge. Nevertheless, for our goal of simply estimating the typical merging times required by these seed models to reproduce the observations, a simple model with fixed delay time suffices. As we can see, the time-delay causes the merger rates at the highest redshifts ($z \gtrsim 10$) to be strongly suppressed. Because all these earliest mergers are pushed to later times, the merger rates are enhanced at lower redshifts.

Since the BH growth is merger-dominated, the corrected final mass of a BH at a given redshift snapshot $z$ is then given by

$$M_{\rm bh}(z) = N_{\rm prog}(z, \tau) \times M_{\rm seed}, \quad (4)$$

where $N_{\rm prog}(z, \tau)$ is the number of progenitors contributed by all merger events before redshift $z$ for a given delay time $\tau$. In Fig. 14, we show the impact of different delay times on the $M_*$ versus $M_{\rm bh}$ relations at $z = 5$ for the SM5 and SM5_LW10 seed models in the unconstrained simulations. Not surprisingly, the time-delay

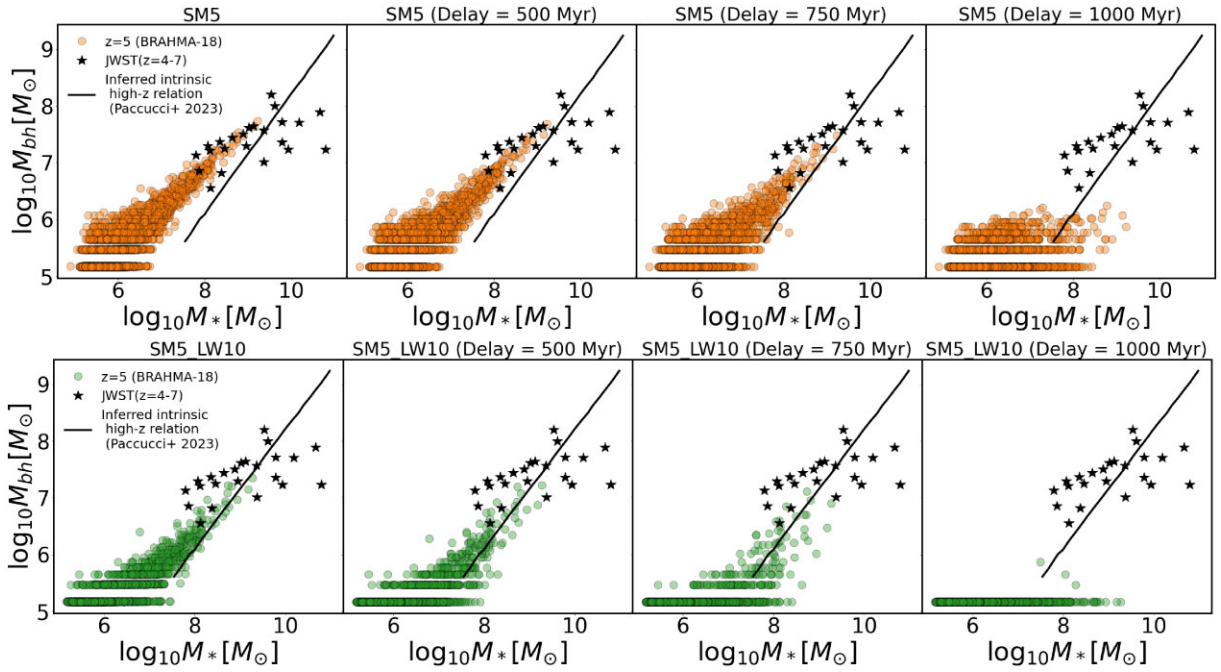


**Figure 14.** Revised $z = 5 M_*$–$M_{\rm bh}$ relations for simulations with the two most lenient seed models SM5 and SM5_LW10, under different assumptions of delay times. The leftmost panel assumes no delay time, the remaining panels assume non-zero delay time. These are shown for the unconstrained simulations. Since accretion driven BH growth is negligible, $M_{\rm bh}$ is calculated by simply multiplying the seed mass by the number of merger progenitors before $z = 5$. To produce BHs with masses similar to the *JWST* AGNs, the delay times need to be $\lesssim$ 750 Myr.

decreases the BH masses accumulated at $z = 5$, as the mergers that are delayed to $z < 5$ no longer contribute to the $z = 5$ BH mass. The SM5_LW10 seed model continues to be consistent with the P23 relation up to a delay time of 750 Myrs. But for a delay time of 1000 Myrs, the predicted BH masses are strongly suppressed to values significantly below the *JWST* measurements. This is a direct consequence of the fact that the peak seed formation time is $z \sim 12$, implying that a delay time of $\gtrsim$ 1000 Myrs would lead to most mergers happening at $z \lesssim 5$ (revisit Fig. 13).

Overall, we find that for our most optimistic seed models, we would be able to reproduce the current *JWST* measurements if the delay times between BH mergers and galaxy mergers are $\lesssim$ 750 Myr. However, the delay times at these high redshifts are highly uncertain, and several recent works are finding that it is difficult to sink BHs to the halo centres within low mass halos at high redshifts (Tremmel et al. 2018; Bellovary et al. 2021; Ma et al. 2021; Ricarte et al. 2021; Partmann et al. 2023). Even at low redshifts, it is not clear whether SMBH pairs are able to effectively harden once they are at separations below a few parsecs; this is commonly known as the 'final parsec problem' (Begelman, Blandford & Rees 1980; Milosavljević & Merritt 2003). Nevertheless, mechanisms such as drag to circumbinary gas disks, stellar loss cone scattering and BH triple interactions could potentially solve the final parsec problem. To that end, recent detection of the stochastic gravitational wave background by the various Pulsar Timing Array (PTA) collaborations such as North American Nanohertz Observatory for Gravitational Waves (NANOGrav, Agazie et al. 2023), European and Indian PTA (EPTA + InPTA, Antoniadis et al. 2024), Chinese PTA (CPTA, Xu et al. 2023), and the Parkes PTA (PPTA; Reardon et al. 2023) serve as the first possible hint that SMBHs do merge. In the future, we will trace the subresolution dynamics of our inspiraling BHs and investigate the role of these processes at high redshifts. We will do this using post-processing models similar to the ones developed in Kelley et al. (2017), and thereby estimate these merging delay times.

### 3.9 Predictions at cosmic noon: implications of recently observed $z \sim$ 1–3 overmassive BHs

While this paper largely focuses on the $z \sim$ 4–7 BH populations, very recently, Mezcua et al. (2024) reported *JWST* observations of 12 SMBHs at $z \sim$ 1–3 that are also overmassive compared to the local scaling relations. In Fig. 15, we compare these observations to our unconstrained simulation predictions at the $z = 2$ snapshot for all the seed models. We find that even for the most optimistic seed model (SM5) under zero delay time for the BH mergers ($\tau = 0$), the predicted $M_* - M_{\rm bh}$ relations are already very close to the local measurements at $z = 2$. Therefore, while *JWST* observes $\sim 10^7$–$10^9$ M$_\odot$ BHs within galaxies with stellar masses $\sim 10^9$ M$_\odot$, the SM5 model predicts $\sim 10^6$–$10^7$ M$_\odot$ BHs within similarly massive simulated galaxies. The strictest SM5_LW10_LOWSPIN_RICH seed model predicts BHs that are even smaller than SM5 by a factor of $\sim$ 10. Overall, because galaxy growth is significantly faster than BH growth between $z \sim 4$ and $z \sim 2$ in our simulations, none of our seed models (including the most optimistic one) produce BHs that overlap the overmassive BHs at cosmic noon reported by Mezcua et al. (2024).

As with the $z \sim$ 4–7 AGNs, the BH mass measurements of the cosmic noon AGN populations may also be impacted by Lauer bias and Eddington bias. Here again, our simulations are not large enough to produce any substantially up-scattered BHs that are significantly above the mean relations. Given the 1.5–2 dex scatter in the TNG300 simulation (grey points in Fig. 15), we could expect the SM5 seed model to produce a significant number of up-scattered BHs consistent with the Mezcua et al. (2024) observations if it was run over a larger volume. However, for the most restrictive

SM5_LW10_LOWSPIN_RICH seed model, wherein the mean relation is $\sim 2$ dex below the observations, it would very difficult to produce BHs up-scattered enough to overlap with the observations even in a TNG300-like volume. Here again, recall that the *JWST* surveys are substantially smaller than TNG300. Overall, the detection of these overmassive $z \sim 1$–3 BHs further adds to our longstanding puzzle of SMBH origins particularly at high-$z$, as they are even more difficult to produce with our seed models than the $z \sim 4$–7 *JWST* AGN and the $z \gtrsim 6$ pre-*JWST* quasars (see Bhowmick et al. 2022b). This further echoes the need to explore alternative BH seeding and growth scenarios described at the end of Section 3.7.

## 4 SUMMARY AND CONCLUSIONS

Recent *JWST* measurements hint at the possible existence of overmassive BHs that are $\sim 10$–100 times higher on the $M_*$ versus $M_{\rm bh}$ plane compared to the local scaling relations. To understand the possible implications of these developments on BH seeding, we have studied the growth of SMBHs at high redshift ($z \sim 4$–7) under systematic variations of heavy seeding scenarios by running a set of cosmological hydrodynamic simulations as part of the BRAHMA suite. To emulate heavy seeding scenarios, we placed $1.5 \times 10^5$ M$_\odot$ seeds using novel seeding prescriptions motivated from DCBH formation conditions. Our prescriptions identified seed forming halos using combinations of several seeding criteria that include (1) sufficient amount of dense and metal-poor gas (5 times the seed mass), (2) sufficient LW radiation ($\gtrsim 10$ $J_{21}$), (3) low enough gas spins (less than the Toomre instability threshold), and (4) sufficiently rich environments (at least one neighbouring halo of comparable or higher mass) where one can expect dynamical heating due to major mergers. We ran simulations that sequentially stacked the above seeding criteria and studied their impact on the high-$z$ BH populations in the context of the *JWST* results. Our main conclusions are summarized as follows.

### 4.1 Seed models have no significant impact on high-$z$ galaxy populations and AGN LFs: these predictions are also broadly consistent with observations

Notably, our seed models have a negligible consequence on the galaxy populations. This is likely because the BH accretion rates are too small for AGN feedback to impact the galaxies. Additionally, the seed models also do not significantly impact the relatively bright end ($L_{\rm bol} \gtrsim 10^{43}$ erg s$^{-1}$) of our simulated AGN populations. As also noted in our previous papers, this is because regardless of how many seeds are produced, there are only a limited set of environments that support enough gas accretion to produce luminous AGN. Concurrently, we also find that the simulations are in broad agreement with *JWST* galaxy and AGN populations for the galaxy LFs, galaxy stellar mass functions, as well as the AGN LFs. This is particularly encouraging as it not only serves as a validation, but also as a benchmark to understand the implications of measurements that are much more challenging to observationally probe for the *JWST* AGNs and their host galaxies, for example the $M_{\rm bh}$ versus $M_*$ relations.

### 4.2 Simulations do not overlap with the *JWST* observations on the galaxy stellar mass versus AGN luminosity plane

Despite the simulations being in simultaneous agreement with the galaxy stellar mass functions as well as the AGN LFs, the simulated AGNs do not overlap with the *JWST* AGNs on the $M_*$ versus $L_{\rm bol}$ plane. More specifically, the simulated AGNs with

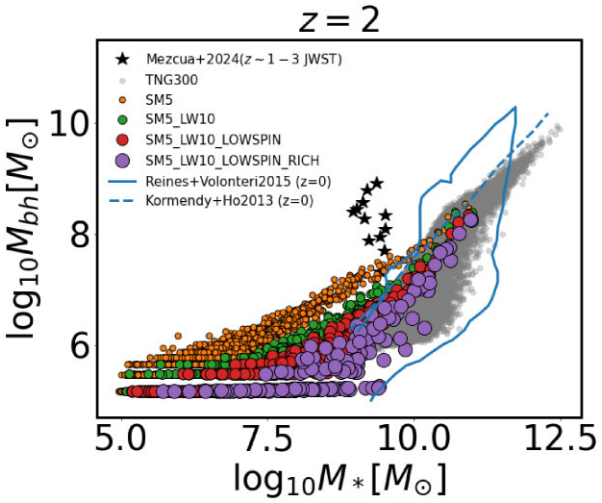


**Figure 15.** $M_*$–$M_{\rm bh}$ relations at $z = 2$ produced by our unconstrained simulations compared against the recent observations of overmassive BHs at cosmic noon (Mezcua et al. 2024) with the assumption of zero delay time. Our simulated BHs are close to the local scaling relations by $z \sim 2$ for all the seed models. Therefore, the simulated BHs are significantly smaller than the *JWST* observations for all the seed models.

$L_{\rm bol} \gtrsim 10^{44}$ erg s$^{-1}$ live in $M_* \gtrsim 10^9$ M$_\odot$ galaxies, which are $\sim 10$ times higher than the measured stellar masses of the *JWST* AGN hosts. Importantly, this discrepancy is independent of the potential uncertainties in the observed BH masses. Possible reasons for this discrepance include (1) AGN variability at short time-scales could lead to Eddington bias, i.e. their preferential detection at luminosities significantly higher than their *time averaged values*. (2) Potential underestimation of the observed stellar masses due to the difficulty in subtracting the AGN contribution from the observed light. Lastly, (3) due to Lauer bias, we may preferentially observe only the significantly up-scattered AGN having luminosities significantly higher than the mean $M_*$ versus $L_{\rm bol}$ relation; however, this would imply that the scatter in the $M_*$ versus $L_{\rm bol}$ relations is significantly higher than the predictions from the simulations.

### 4.3 BH growth at high-$z$ is dominated by mergers: therefore, BH masses are substantially impacted by the seed model

In our simulations, the BH growth is predominantly contributed by mergers at these high redshifts, with accretion driven BH growth being relatively small. Due to this, our seed models have a substantial impact on the BH masses even though the AGN luminosities are minimally impacted. To that end, by repositioning the BHs to the local potential minima, we assume the most optimistic scenario for the merging efficiencies wherein there is zero time delay between BH mergers and galaxy mergers. As we explain next, despite this assumption, our restrictive seed models significantly underpredict the $M_*$ versus $M_{\rm bh}$ relations compared to *JWST*.

### 4.4 Comparing the simulation predictions against the *JWST* measurements on the $M_*$ versus $M_{\rm bh}$ plane

Amongst our seed models, only the optimistic ones without the gas spin and environment based criteria (SM5 and SM5_LW10) produce BHs that have some overlap with the *JWST* AGNs on the $M_*$ versus $M_{\rm bh}$ plane. On the other hand, for the two restrictive seed models (SM5_LW10_LOWSPIN and SM5_LW10_LOWSPIN_RICH), the predictions are substantially below the *JWST* AGNs. However,

if the Lauer bias is substantial in the observed BH populations, the resulting BH masses may also be significantly up-scattered on the $M_*$ versus $M_{\rm bh}$ plane, as more massive BHs typically power more luminous AGN. This makes it difficult to directly compare these results with the BRAHMA boxes since they are not large enough to produce BHs that are substantially up-scattered.

### 4.5 Comparing the simulation predictions against the intrinsic high-$z$ $M_*$ versus $M_{\rm bh}$ relation derived by P23

P23 found that even after accounting for possible systematic biases and measurement uncertainties in the BH mass and host stellar masses, the *JWST* AGNs (as they currently stand) implied an intrinsic $M_*$ versus $M_{\rm bh}$ relation that lies above the local scaling relations at a $> 3\sigma$ confidence level. Making an 'apples-to-apples' comparison of this high-$z$ relation against the simulations, provides strong implications on our seed models. For our most restrictive seed model (SM5_LW10_LOWSPIN_RICH), the BH masses are lower than the P23 relation by a factor of $\sim 10$ at $z = 4$ & 5. This is because not enough seeds are produced to fuel the merger driven BH growth. In addition, any time-delay between BH mergers and galaxy mergers would further compromise the growth of these BHs. Therefore, if the inferred high-$z$ $M_*$ versus $M_{\rm bh}$ relation from P23 proves to be robust in the future (when we have larger samples of high-$z$ AGN), this could potentially rule out heavy seeds formed via standard direct collapse scenarios (as considered in this paper) as their sole seeding origins.

Only the simulation (SM5_LW10) that excludes the gas spin and environmental richness criteria, predicts a $M_*$ versus $M_{\rm bh}$ relation consistent with the P23 relation. If we also exclude the LW flux criterion (SM5), the simulation overpredicts the BH masses compared to the P23 relation. However, these simulations are rather optimistic. For example, not all regions with sufficient dense and metal-poor gas are expected to form DCBHs (as assumed by the SM5 simulation). This is because the molecular hydrogen will cool and fragment the gas to form Pop III stars instead. Moreover, even when we include the LW flux criterion to restrict seeding to those halos wherein the radiation can suppress the molecular Hydrogen cooling, our choice of $J_{\rm crit} = 10\ J_{21}$ is much lower than the predictions from small scale hydrodynamic simulations ($\gtrsim 1000\ J_{21}$). While such low $J_{\rm crit}$ values may be feasible if the gas is subjected to dynamical heating during halo mergers, restricting the seed formation to rich environments (where these major mergers are expected to occur) leads to BHs significantly less massive than the P23 relation.

We further determined that even with our most optimistic simulations (SM5 and SM5_LW10), one could potentially produce the *JWST* AGNs and the P23 relation only if the typical delay times between the BH mergers and galaxy mergers are $\lesssim 750$ Myr. However, several recent works are finding that sinking BHs to halo centres is challenging within low mass halos at high redshifts (Ma et al. 2021; Partmann et al. 2023). Additionally, at low redshifts, the estimated delay times for the merger events can be up to several Gyr (Kelley et al. 2017). Therefore, the feasibility of delay times being $\lesssim 750$ Myr at higher redshifts will require further investigation in the future.

### 4.6 Possibility of systematic biases in the BH mass measurements would imply that the simulations underpredict the scatter in the BH–galaxy scaling relations.

Our work also reveals that the BH mass and host stellar mass measurements of these high-$z$ *JWST* AGNs may have significant implications not just on the mean trends, but also the underlying scatter within the high-$z$ $M_*$ versus $M_{\rm bh}$ (and $M_*$ versus $L_{\rm bol}$) relations. In general, having a larger scatter in the intrinsic scaling relations enhances the likelihood of detecting up-scattered objects in smaller volume surveys. Therefore, if the *JWST* BH mass measurements are indeed up-scattered due to Lauer bias and Eddington bias, it would imply that the high-$z$ scatter is significantly larger than predicted by our simulations. Due to the limited volume, the BRAHMA boxes do not effectively probe the full scatter of the $M_*$ versus $M_{\rm bh}$ relations, as they cannot capture the formation of rare up-scattered BHs. In the future, we plan to explore the scatter in more detail by running some of our seed models within much larger simulation volumes.

### 4.7 Final remarks

Overall, our work hints that if the high-$z$ BH populations are indeed confirmed to be systematically overmassive than the local scaling relations, this will have profound implications on BH seeding. More specifically, we show that while heavy $\sim 10^5$ $M_\odot$ seeds can produce these overmassive BH populations, their formation needs to be more efficient than the scenarios typically considered for DCBHs. While our simulation boxes already produce heavy seeds in higher numbers than typically assumed, there may also be alternative heavy seeding channels that may be more efficient than the ones considered in this work. For instance, in this work, the seeding efficiency is limited by the mass resolution of the seed forming halos and the eEOS description of the ISM; this prevents us from exploring seed formation in halos that are significantly below our halo mass resolution limit of $\sim 5 \times 10^7$ $M_\odot$. However, higher resolution simulations with an explicitly resolved ISM will allow us to explore heavy seed formation in lower mass halos. Additionally, light seeds are expected to form in much higher numbers compared to heavy seeds. These light seeds could also potentially boost the merger driven BH growth of heavy seeds. Another possibility is that the initial seed masses could be much higher than $\sim 10^5$ $M_\odot$. For example, Mayer et al. (2024) demonstrated that dynamical heating caused by major mergers could lead to direct formation of $\sim 10^8$ $M_\odot$ BHs even in metal enriched regions that are concurrently undergoing starbursts. Finally, the assembly of overmassive high-$z$ BHs could be driven by a select few seeds that grow much more rapidly via more efficient gas accretion channels compared to the Bondi-accretion model considered in this work (Jeon et al. 2024). In the near future, we plan to explore all above avenues in detail and investigate the joint implications of possible high-$z$ overmassive BHs on seeding, growth, and dynamics.

## DATA AVAILABLITY

The underlying data used in this work shall be made available upon reasonable request to the corresponding author.

## ACKNOWLEDGEMENTS

LB acknowledges support from NSF awards AST-1909933 and AST-2307171 and Cottrell Scholar Award #27553 from the Research Corporation for Science Advancement. PT acknowledges support from NSF-AST 2008490. RW acknowledges funding of a Leibniz Junior Research Group (project number J131/2022). LH acknowledges support by the Simons Collaboration on 'Learning the Universe'.

## REFERENCES

Agarwal B., Davis A. J., Khochfar S., Natarajan P., Dunlop J. S., 2013, MNRAS, 432, 3438

Agazie G. et al., 2023, ApJ, 951, L8
Akins H. B. et al., 2024, preprint (arXiv:2406.10341)
Amaro-Seoane P. et al., 2017, preprint (arXiv:1702.00786)
Andika I. T. et al., 2024, A&A, 685, A25
Antoniadis J. et al., 2024, A&A, 685, A94
Bañados E. et al., 2018, Nature, 553, 473
Baggen J. F. W. et al., 2023, ApJ, 955, L12
Barnes J., Hut P., 1986, Nature, 324, 446
Bañados E. et al., 2016, ApJS, 227, 11
Begelman M. C., 2010, MNRAS, 402, 673
Begelman M. C., Silk J., 2023, MNRAS, 526, L94
Begelman M. C., Blandford R. D., Rees M. J., 1980, Nature, 287, 307
Begelman M. C., Volonteri M., Rees M. J., 2006, MNRAS, 370, 289
Bellovary J. M., Cleary C. E., Munshi F., Tremmel M., Christensen C. R., Brooks A., Quinn T. R., 2019, MNRAS, 482, 2913
Bellovary J. M. et al., 2021, MNRAS, 505, 5129
Bhowmick A. K. et al., 2021, MNRAS, 507, 2012
Bhowmick A. K., Blecha L., Torrey P., Kelley L. Z., Vogelsberger M., Nelson D., Weinberger R., Hernquist L., 2022a, MNRAS, 510, 177
Bhowmick A. K. et al., 2022b, MNRAS, 516, 138
Bhowmick A. K., Blecha L., Torrey P., Weinberger R., Kelley L. Z., Vogelsberger M., Hernquist L., Somerville R. S., 2024a, MNRAS, 529, 3768
Bhowmick A. K. et al., 2024b, MNRAS, 531, 4311
Blecha L., Loeb A., 2008, MNRAS, 390, 1311
Blecha L. et al., 2016, MNRAS, 456, 961
Bogdán Á. et al., 2024, Nat. Astron., 8, 126
Bouwens R. J., Illingworth G. D., van Dokkum P. G., Oesch P. A., Stefanon M., Ribeiro B., 2022a, ApJ, 927, 81
Bouwens R. J., Illingworth G., Ellis R. S., Oesch P., Stefanon M., 2022b, ApJ, 940, 55
Bromm V., Loeb A., 2003, ApJ, 596, 34
Chabrier G., 2003, PASP, 115, 763
Das A., Schleicher D. R. G., Basu S., Boekholt T. C. N., 2021a, MNRAS, 505, 2186
Das A., Schleicher D. R. G., Leigh N. W. C., Boekholt T. C. N., 2021b, MNRAS, 503, 1051
Davies M. B., Miller M. C., Bellovary J. M., 2011, ApJ, 740, L42
Davis M., Efstathiou G., Frenk C. S., White S. D. M., 1985, ApJ, 292, 371
DeGraf C., Sijacki D., 2020, MNRAS, 491, 4973
Denney K. D., 2012, ApJ, 759, 44
Di Matteo T., Khandai N., DeGraf C., Feng Y., Croft R. A. C., Lopez J., Springel V., 2012, ApJ, 745, L29
Dijkstra M., Haiman Z., Mesinger A., Wyithe J. S. B., 2008, MNRAS, 391, 1961
Ding X. et al., 2023, Nature, 621, 51
Donnari M. et al., 2019, MNRAS, 485, 4817
Dunn G., Holley-Bockelmann K., Bellovary J., 2020, ApJ, 896, 72
Durodola E., Pacucci F., Hickox R. C., 2024, preprint (arXiv:2406.10329)
Fan X. et al., 2001, AJ, 122, 2833
Feng Y., Di-Matteo T., Croft R. A., Bird S., Battaglia N., Wilkins S., 2016, MNRAS, 455, 2778
Ferrara A., Salvadori S., Yue B., Schleicher D., 2014, MNRAS, 443, 2410
Finkelstein S. L. et al., 2023, ApJ, 946, L13
Fryer C. L., Woosley S. E., Heger A., 2001, ApJ, 550, 372
Genel S. et al., 2018, MNRAS, 474, 3976
Gerosa D., Moore C. J., 2016, Phys. Rev. Lett., 117, 011101
Greene J. E., Ho L. C., 2005, ApJ, 630, 122
Greene J. E. et al., 2024, ApJ, 964, 39
Habouzit M., Volonteri M., Latif M., Dubois Y., Peirani S., 2016, MNRAS, 463, 529
Habouzit M., Volonteri M., Dubois Y., 2017, MNRAS, 468, 3935
Habouzit M. et al., 2019, MNRAS, 484, 4413
Habouzit M. et al., 2021, MNRAS, 503, 1940
Habouzit M. et al., 2022, MNRAS, 509, 3015
Haemmerlé L., Klessen R. S., Mayer L., Zwick L., 2021, A&A, 652, L7
Hahn O., Abel T., 2011, MNRAS, 415, 2101
Harikane Y. et al., 2022, ApJS, 259, 20
Harikane Y. et al., 2023, ApJ, 959, 39
Holley-Bockelmann K., Gültekin K., Shoemaker D., Yunes N., 2008, ApJ, 686, 829
Hosokawa T., Omukai K., Yorke H. W., 2012, ApJ, 756, 93
Hosokawa T., Yorke H. W., Inayoshi K., Omukai K., Yoshida N., 2013, ApJ, 778, 178
Huang K.-W., Di Matteo T., Bhowmick A. K., Feng Y., Ma C.-P., 2018, MNRAS, 478, 5063
Jeon J., Bromm V., Liu B., Finkelstein S. L., 2024, preprint (arXiv:2402.18773)
Jiang L. et al., 2016, ApJ, 833, 222
Kannan R., Vogelsberger M., Pfrommer C., Weinberger R., Springel V., Hernquist L., Puchwein E., Pakmor R., 2017, ApJ, 837, L18
Kannan R., Garaldi E., Smith A., Pakmor R., Springel V., Vogelsberger M., Hernquist L., 2022, MNRAS, 511, 4005
Kannan R. et al., 2023, MNRAS, 524, 2594
Katz N., Weinberg D. H., Hernquist L., 1996, ApJS, 105, 19
Kaviraj S. et al., 2017, MNRAS, 467, 4739
Kelley L. Z., Blecha L., Hernquist L., 2017, MNRAS, 464, 3131
Kelly B. C., Treu T., Malkan M., Pancoast A., Woo J.-H., 2013, ApJ, 779, 187
Khandai N., Di Matteo T., Croft R., Wilkins S., Feng Y., Tucker E., DeGraf C., Liu M.-S., 2015, MNRAS, 450, 1349
Killi M. et al., 2023, preprint (arXiv:2312.03065)
Kocevski D. D. et al., 2023, ApJ, 954, L4
Kocevski D. D. et al., 2024, preprint (arXiv:2404.03576)
Kokorev V. et al., 2023, ApJ, 957, L7
Kokorev V. et al., 2024, ApJ, 968, 38
Kormendy J., Ho L. C., 2013, ARA&A, 51, 511
Kroupa P., Subr L., Jerabkova T., Wang L., 2020, MNRAS, 498, 5652
Langeroodi D., Hjorth J., 2023, ApJ, 957, L27
Larson R. L. et al., 2023, ApJ, 953, L29
Latif M. A., Schleicher D. R. G., Hartwig T., 2016, MNRAS, 458, 233
Lauer T. R., Tremaine S., Richstone D., Faber S. M., 2007, ApJ, 670, 249
Li Y. et al., 2020, ApJ, 895, 102
Li J. et al., 2024, preprint (arXiv:2403.00074)
Lodato G., Natarajan P., 2006, MNRAS, 371, 1813
Luo Y., Ardaneh K., Shlosman I., Nagamine K., Wise J. H., Begelman M. C., 2018, MNRAS, 476, 3523
Luo Y., Shlosman I., Nagamine K., Fang T., 2020, MNRAS, 492, 4917
Lupi A., Colpi M., Devecchi B., Galanti G., Volonteri M., 2014, MNRAS, 442, 3616
Ma L., Hopkins P. F., Ma X., Anglés-Alcázar D., Faucher-Giguère C.-A., Kelley L. Z., 2021, MNRAS, 508, 1973
Madau P., Dickinson M., 2014, ARA&A, 52, 415
Madau P., Rees M. J., 2001, ApJ, 551, L27
Maiolino R. et al., 2023, preprint (arXiv:2308.01230)
Marinacci F. et al., 2018, MNRAS, 480, 5113
Matsuoka Y. et al., 2018, ApJS, 237, 5
Matsuoka Y. et al., 2019, ApJ, 872, L2
Matthee J. et al., 2024, ApJ, 963, 129
Mayer L., Capelo P. R., Zwick L., Di Matteo T., 2024, ApJ, 961, 76
Mezcua M., Pacucci F., Suh H., Siudek M., Natarajan P., 2024, ApJ, 966, L30
Milosavljević M., Merritt D., 2003, ApJ, 596, 860
Mortlock D. J. et al., 2011, Nature, 474, 616
Naiman J. P. et al., 2018, MNRAS, 477, 1206
Natarajan P., Volonteri M., 2012, MNRAS, 422, 2051
Natarajan P., Pacucci F., Ferrara A., Agarwal B., Ricarte A., Zackrisson E., Cappelluti N., 2017, ApJ, 838, 117
Natarajan P., Pacucci F., Ricarte A., Bogdán Á., Goulding A. D., Cappelluti N., 2024, ApJ, 960, L1
Navarro-Carrera R., Rinaldi P., Caputi K. I., Iani E., Kokorev V., van Mierlo S. E., 2024, ApJ, 961, 207
Nelson D. et al., 2015, Astron. Comput., 13, 12
Nelson D. et al., 2018, MNRAS, 475, 624
Nelson D. et al., 2019a, Comput. Astrophys. Cosmol., 6, 2
Nelson D. et al., 2019b, MNRAS, 490, 3234
Ni Y., Di Matteo T., Feng Y., 2022, MNRAS, 509, 3043

Onoue M. et al., 2023, ApJ, 942, L17
Pacucci F., Loeb A., 2024, ApJ, 964, 154
Pacucci F., Nguyen B., Carniani S., Maiolino R., Fan X., 2023, ApJ, 957, L3
Pakmor R., Bauer A., Springel V., 2011, MNRAS, 418, 1392
Pakmor R., Pfrommer C., Simpson C. M., Kannan R., Springel V., 2016, MNRAS, 462, 2603
Pakmor R. et al., 2023, MNRAS, 524, 2539
Partmann C., Naab T., Rantala A., Genina A., Mannerkoski M., Johansson P. H., 2023, preprint (arXiv:2310.08079)
Pérez-González P. G. et al., 2024, ApJ, 968, 4
Pillepich A. et al., 2018a, MNRAS, 473, 4077
Pillepich A. et al., 2018b, MNRAS, 475, 648
Pillepich A. et al., 2019, MNRAS, 490, 3196
Planck Collaboration XIII, 2016, A&A, 594, A13
Ponti G., Papadakis I., Bianchi S., Guainazzi M., Matt G., Uttley P., Bonilla N. F., 2012, A&A, 542, A83
Ramos Padilla A. F., Ashby M. L. N., Smith H. A., Martínez-Galarza J. R., Beverage A. G., Dietrich J., Higuera-G. M.-A., Weiner A. S., 2020, MNRAS, 499, 4325
Reardon D. J. et al., 2023, ApJ, 951, L6
Reed S. L. et al., 2017, MNRAS, 468, 4702
Regan J. A., Johansson P. H., Wise J. H., 2014, ApJ, 795, 137
Regan J. A., Haiman Z., Wise J. H., O'Shea B. W., Norman M. L., 2020a, Open J. Astrophys., 3, E9
Regan J. A., Wise J. H., Woods T. E., Downes T. P., O'Shea B. W., Norman M. L., 2020b, Open J. Astrophys., 3, 15
Regan J. A., Wise J. H., O'Shea B. W., Norman M. L., 2020c, MNRAS, 492, 3021
Reines A. E., Volonteri M., 2015, ApJ, 813, 82
Ricarte A., Tremmel M., Natarajan P., Zimmer C., Quinn T., 2021, MNRAS, 503, 6098
Richards G. T. et al., 2011, AJ, 141, 167
Rodriguez-Gomez V. et al., 2019, MNRAS, 483, 4140
Sayeb M., Blecha L., Kelley L. Z., Gerosa D., Kesden M., Thomas J., 2021, MNRAS, 501, 2531
Schleicher D. R. G., Palla F., Ferrara A., Galli D., Latif M., 2013, A&A, 558, A59
Scoggins M. T., Haiman Z., 2024, MNRAS, 531, 4584
Scoggins M. T., Haiman Z., Wise J. H., 2023, MNRAS, 519, 2155
Shang C., Bryan G. L., Haiman Z., 2010, MNRAS, 402, 1249
Shen X., Hopkins P. F., Faucher-Giguère C.-A., Alexander D. M., Richards G. T., Ross N. P., Hickox R. C., 2020, MNRAS, 495, 3252
Shen X., Vogelsberger M., Boylan-Kolchin M., Tacchella S., Kannan R., 2023, MNRAS, 525, 3254
Sijacki D., Vogelsberger M., Genel S., Springel V., Torrey P., Snyder G. F., Nelson D., Hernquist L., 2015, MNRAS, 452, 575
Siwek M., Weinberger R., Hernquist L., 2023, MNRAS, 522, 2707
Siwek M., Kelley L. Z., Hernquist L., 2024, preprint (arXiv:2403.08871)
Smith B., Sigurdsson S., Abel T., 2008, MNRAS, 385, 1443
Smith B. D., Regan J. A., Downes T. P., Norman M. L., O'Shea B. W., Wise J. H., 2018, MNRAS, 480, 3762
Springel V., 2010, MNRAS, 401, 791
Springel V., Hernquist L., 2003, MNRAS, 339, 289
Springel V., White S. D. M., Tormen G., Kauffmann G., 2001, MNRAS, 328, 726
Springel V. et al., 2018, MNRAS, 475, 676
Stone M. A., Lyu J., Rieke G. H., Alberts S., Hainline K. N., 2024, ApJ, 964, 90
Sugimura K., Omukai K., Inoue A. K., 2014, MNRAS, 445, 544
Taylor P., Kobayashi C., 2015, MNRAS, 448, 1835
Terrazas B. A., Bell E. F., Henriques B. M. B., White S. D. M., Cattaneo A., Woo J., 2016, ApJ, 830, L12
Torrey P. et al., 2019, MNRAS, 484, 5587
Tremmel M., Karcher M., Governato F., Volonteri M., Quinn T. R., Pontzen A., Anderson L., Bellovary J., 2017, MNRAS, 470, 1121
Tremmel M., Governato F., Volonteri M., Pontzen A., Quinn T. R., 2018, ApJ, 857, L22
Übler H. et al., 2021, MNRAS, 500, 4597
Übler H. et al., 2023, A&A, 677, A145
Venemans B. P. et al., 2015, MNRAS, 453, 2259
Visbal E., Haiman Z., 2018, ApJ, 865, L9
Vogelsberger M., Genel S., Sijacki D., Torrey P., Springel V., Hernquist L., 2013, MNRAS, 436, 3031
Vogelsberger M. et al., 2014a, MNRAS, 444, 1518
Vogelsberger M. et al., 2014b, Nature, 509, 177
Vogelsberger M., Marinacci F., Torrey P., Puchwein E., 2020a, Nature Rev. Phys., 2, 42
Vogelsberger M. et al., 2020b, MNRAS, 492, 5167
Volonteri M., Madau P., 2008, ApJ, 687, L57
Wang F. et al., 2018, ApJ, 869, L9
Wang F. et al., 2021, ApJ, 907, L1
Weibel A. et al., 2024, preprint (arXiv:2403.08872)
Weinberger R. et al., 2017, MNRAS, 465, 3291
Weinberger R. et al., 2018, MNRAS, 479, 4056
Weinberger R., Springel V., Pakmor R., 2020, ApJS, 248, 32
Willott C. J. et al., 2010, AJ, 139, 906
Wise J. H., Regan J. A., O'Shea B. W., Norman M. L., Downes T. P., Xu H., 2019, Nature, 566, 85
Wolcott-Green J., Haiman Z., Bryan G. L., 2017, MNRAS, 469, 3329
Xu H., Wise J. H., Norman M. L., 2013, ApJ, 773, 83
Xu H. et al., 2023, Res. Astron. Astrophys., 23, 075024
Yang J. et al., 2019, AJ, 157, 236
Yue B., Ferrara A., Salvaterra R., Xu Y., Chen X., 2014, MNRAS, 440, 1263
Yue M. et al., 2024, ApJ, 966, 176
Zinger E. et al., 2020, MNRAS, 499, 768

This paper has been typeset from a TEX/LATEX file prepared by the author.